THE ASTROPHYSICAL JOURNAL, 454:254–276, 1995 November 20

THE FRAGMENTATION AND VAPORIZATION OF DUST IN GRAIN-GRAIN COLLISIONS

KAZIMIERZ J. BORKOWSKI[1]
Universities Space Research Association, Laboratory for Astronomy and Solar Physics, NASA/Goddard Space Flight Center, and Department of Astronomy, University of Maryland, College Park, MD 20742

AND

ELI DWEK
Laboratory for Astronomy and Solar Physics, NASA/Goddard Space Flight Center, Greenbelt, MD 20771
Received 1994 December 27; accepted 1995 June 1

ABSTRACT

We present a detailed analysis of the evolution of the size distribution of fast-moving interstellar dust particles decelerating in a dusty plasma. The physical processes considered in this paper include sputtering by gas-grain collisions, and partial and complete evaporation, fragmentation, and cratering by grain-grain collisions. We find that the final distribution of grains, initially characterized by a power-law distribution in grain sizes, exhibits an excess of small-to-large particles, compared to the initial distribution. This excess depends on the initial grain velocity and should be detectable by infrared observations of low- and intermediate-velocity clouds with the *Infrared Space Observatory* scheduled for launch around 1996.

Subject heading: dust, extinction

1. INTRODUCTION

The shock processing of interstellar grains by sputtering or grain-grain collisions plays an important role in the recycling of condensable elements back into the gas phase, and in modifying the grain size distribution. The physical mechanisms behind these processes have been investigated by numerous authors (Burke & Silk 1974; Shull 1977, 1978; Barlow 1978a,b; Draine & Salpeter 1979a; see Dwek & Arendt 1992 for a more extended list of references), and most recently by Tielens et al. (1994), who presented a detailed application of the theory of shock wave propagation in solids to the physics of grain-grain collisions. Shock processing of interstellar grains has various important observational consequences, affecting the elemental depletions in shocked clouds or behind shocks (e.g., Spitzer 1976; Barlow & Silk 1977; Cowie 1978; Shull 1978; Seab & Shull 1983; Jones et al. 1994; Dwek, Foster, & Vancura 1994); the UV extinction of stars seen through a shocked gas (Seab & Shull 1983); the ionization structure and X-ray emission behind fast shocks (Itoh 1989; Vancura et al. 1994); and the general evolution of the dust and the depletion of elements in the interstellar medium (Barlow 1978c; Dwek & Scalo 1979, 1980; Draine & Salpeter 1979b; McKee et al. 1987; McKee 1989). The catastrophic fragmentation of grains in grain-grain collisions plays a particularly important role in determining the initial grain size distribution in their formation sites (Biermann & Harwit 1980) and in the general interstellar medium (Liffman 1990).

An important tool for studying grain destruction is examining its effect on the infrared (IR) signature of a shocked gas. In high-velocity shocks, grain destruction is dominated by thermal sputtering, which creates a deficiency of small dust particles compared to the preshock gas. Since small dust particles are stochastically heated in shocked plasmas (Dwek 1986), the effect of grain destruction should be manifested in the short-wavelength emission ($\lambda < 25$ μm) from supernova remnants (Dwek & Arendt 1992, and references therein) and shocks in general (Dwek et al. 1994). In low-velocity shocks ($v < 200$ km s^{-1}), grain fragmentation and vaporization by grain-grain collisions will be the dominant grain processing mechanisms. These processes will create an excess of small dust particles compared to the unshocked gas. These particles will be stochastically heated by the ambient radiation field (Draine & Anderson 1985). Preliminary studies of the IR emission from intermediate-velocity molecular clouds (Heiles, Reach, & Koo 1988) suggest an excess of short-wavelength IR emission over that expected from unshocked clouds that are heated by the intestellar radiation field.

The purpose of this paper is to present a quantitative estimate of the evolution of the distribution of a population of initially fast-moving dust particles as they are decelerated in a dusty plasma. The grain size distribution evolves due to sputtering, complete and partial vaporization, and grain fragmentation. Grain destruction by sputtering is a relatively well understood theory, and well supported by observations (see references in Tielens et al. 1994). In comparison, the vaporization and fragmentation of dust in grain-grain collisions is less understood and suffers from the fact that the experimental data, which are conducted primarily on macroscopic rocks and slabs of material, cannot be readily applied to the realm of submicron interstellar dust particles.

Rather than developing a rigorous, complex theory for the propagation of shocks to develop a prescription for the vaporization of dust as was done by Tielens et al. (1994), we have chosen to adopt an empirical approach to the subject. Based on a variety of experimental and theoretical considerations, we have adopted criteria, characterized by energy thresholds and yields, for the complete and partial vaporization of dust particles, and for their fragmentation as well. An investigation of the physical processes that modify the grain size distribution is presented in § 2. Particular emphasis is placed on the fragmentation and cratering of dust particles, both processes that constitute a source of small dust particles behind the shock. In § 3 we present the rates at which these various processes change the grain size distribution. To do so, we divided the processes

[1] Currently NAS/NRC Senior Research Associate at Laboratory for High Energy Astrophysics, NASA/Goddard Space Flight Center, Code 666, Greenbelt, MD 20771.

into two distinct categories: continuous processes—sputtering and cratering which result in the gradual erosion of the grain radius, and catastrophic processes—partial and complete vaporization and fragmentation which result in the total disruption of a dust particle. The evolution of sizes of a population of interstellar dust particles is cast as an integral equation which is solved for a population of dust particles, characterized by an initial power law in their size distribution, which decelerate from an initial velocity v in a dusty plasma (in § 4). The dust particles that come to rest in the dusty plasma consist of surviving dust grains, decelerated fragments, and very fine dust particles created in cratering collisions, and we present the resulting grain size distribution for several initial grain velocities.

With proper modifications, the formalism developed in this paper can be applied to a variety of astrophysical environments such as low- and intermediate-velocity shocks and dusty stellar outflows (Biermann & Harwit 1980; Jura & Kroto 1990).

2. PHYSICAL PROCESSES MODIFYING THE GRAIN SIZE DISTRIBUTION

2.1. *General Considerations*

Two physical processes that alter the grain size distribution in radiative shocks are sputtering and grain-grain (hereafter g-g) collisions. Sputtering collisions between the grains and the ambient gas result in the ejection of atoms or molecules from the grain. Collisions between the grains can result in the total vaporization of both grains if their relative velocity is high enough. Most collisions, however, result in their partial vaporization and in their breakup into smaller fragments. We will distinguish between two types of g-g collisions: cratering collisions and catastrophic collisions. They are distinguished by the energy deposited in the target grain, the fractional mass in the target grain that is vaporized or fragmented, and the size distribution of the fragments.

A fast collision between dust particles generates a strong shock wave that propagates from the impact site into the solid material. An elementary description of the propagation of shock waves in solids is given by Zeldovich & Raizer (1967), and an application to macroscopic impact cratering is given by Melosh (1989). The passage of a shock compresses the solid and also imparts kinetic energy to the shocked material. In the compression, the molecules (atoms) of the solid are brought into close proximity, increasing the internal energy of the shocked material resulting from the repulsive forces between the atoms. The kinetic and internal energies are about equally partitioned, so about half the shock energy is actually deposited as internal energy in the solid. If the stresses induced by the shock exceed the material strength, the grain material is deformed, crushed, and fragmented. The kinetic energy imparted by the shock to the crushed and fragmented material then removes it out of the impact site. Since the shock strength declines with distance from the impact site, the detailed outcome of the collision will depend (in addition to the properties of the solid such as its density, equation of state, and its compressibility) on the energy of the impact. At low energies, only a limited region around the impact site will be affected by the shock. The propagation of the shock creates a crater, with the excavated material partially ejected from the grain and partially displaced sideways to the crater rim. Most of the mass of the target material remains intact. We will refer to these low-energy g-g collisions as *cratering collisions.* At higher impact energies, the shock energy imparted to the solid exceeds the material strength throughout the grain, and the target grain is broken up into fragments characterized by a wide range of sizes. We will refer to these collisions in which the entire target particle is affected by the collision as *catastrophic collisions.* The grain lifetime and the outcome between these two types of collisions are very different: cratering collisions lead to a gradual decrease in the target grain size, producing a large number of very small fragments, whereas catastrophic collisions lead to the disruption of the entire grain in a single collision, producing fragments with a large range of sizes. Figure 1 is schematic presentation of the grain destruction mechanisms considered in this paper.

The distinction between the two types of collisions is convenient for numerical purposes. It is, however, somewhat artificial, since the transition between these two collision regimes is of course gradual, with intermediate cases giving rise to craters that are comparable in size to that of the target grain. However, cratering collisions constitute an additional source of very small grains in excess of that produced by catastrophic collisions alone. Cratering collisions on graphite grains can be an important source of polycyclic aromatic hydrocarbon (PAH) molecules, generally believed to give rise to the observed mid-infrared interstellar emission features (Allamandola, Tielens, & Barker 1985; Leger & Puget 1984).

A realistic treatment of the process of g-g collisions may therefore require detailed calculations of the propagation of shock waves through solids. Such a detailed treatment is beyond the scope of this paper and premature in light of our poor understanding of the nature of interstellar dust grains, their shape, structure, and composition, and their bulk physical properties. Clearly, grains that are a fluffy aggregate of smaller particles of different composition as envisioned by Mathis & Whiffen (1989) will behave differently than pure spherical graphite or silicate grains. Therefore, our strategy is to understand the basic physical processes that give rise to the various grain destruction processes: sputtering, vaporization, cratering, and catastrophic collisions. Associated with these processes are physical quantities (relevant binding energies, critical stresses, and tensile strengths) that will determine their relative importance. The results of our calculations will therefore depend quite critically on our choice of these parameters. In choosing their values, we will be guided by experimental data, bearing in mind that the available data are strictly applicable to millimeter-size particles, huge by astronomical standards, requiring an extrapolation by more than 3 orders of magnitude. This extrapolation must be done carefully, using theoretical arguments wherever possible. In the following, we will describe the various grain destruction processes in more detail, emphasizing the energy requirements and our treatment of the collision outcome for each case.

2.2. *Sputtering*

The sputtering yield, Y, defined as the average number of sputtered atoms (molecules) per incident projectile particle, is given for projectiles with energy E and normal incidence by (Sigmund 1981; Bohdansky 1984):

$$Y(E, \mu_M) = 0.042\alpha(\mu_M)S_n(E)\zeta(\mu_M, E), \quad (1)$$

were α is an energy independent function of the mass ratio $\mu_M (\equiv M_2/M_1)$ between target atoms in the grain, and incident projectile atoms, $S_n(E)$ is the nuclear stopping power, and $\zeta(\mu_M, E)$ is a correction factor that gives the energy dependence of the

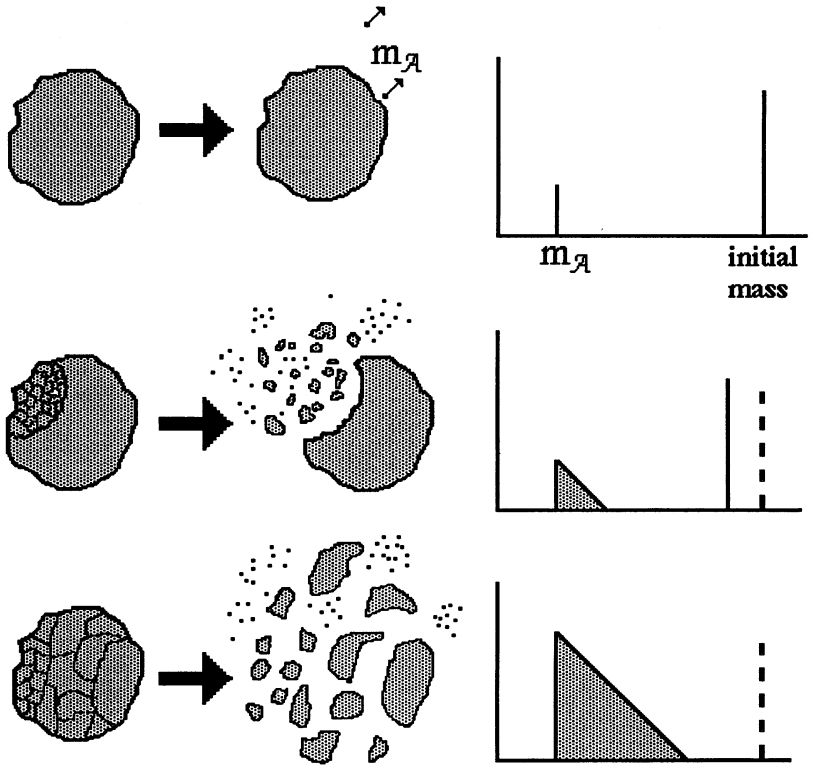

FIG. 1.—A schematic presentation of the various grain destruction mechanisms considered in this paper. Diagrams on the right are sketches of the fragment mass distribution following the destruction event. The mechanisms, from top to bottom, are sputtering, cratering, and catastrophic fragmentation. Partial vaporization (or complete vaporization in the last case) can accompany the last two mechanisms.

sputtering yield near the threshold energy (Bohdansky 1984). The sputtering rate of a dust particle moving with a velocity v through a hot plasma is derived by integrating the sputtering yield over a skewed Maxwellian distribution of gas velocities (Shull 1978). Figures of the sputtering rates in high velocity shocks are presented by Tielens et al. (1994) and Dwek et al. (1994). In compression shocks, the sputtering is mostly a result of the relative motion of the dust through the gas, and the rate is given by

$$\frac{dN}{dt} = \pi a^2 nv\left(1 - \frac{2\phi kT}{mv}\right)Y(E) \quad \text{for } \frac{1}{2}mv^2 > U_s\,, \qquad (2)$$

where U_s is the surface binding energy of the sputtered atom to the grain, a is the grain radius, v is its velocity relative to the gas of temperature T, consisting of atoms of mass m, with a number density n, and $E = \frac{1}{2}mv^2 - \phi kT$, where ϕ is the electric potential on the dust in units of kT. Denoting by $\mathscr{A}$ the atomic number of the atoms (molecules) sputtered off the grains ($\mathscr{A} = 12$ for graphite grains and $\mathscr{A} \approx 20$ for silicates), we can write the rate at which the mass of the grain is eroded by the sputtering as

$$\dot{m}_s = -\mathscr{A}m_H\frac{dN}{dt} = -\pi a^2 \mathscr{A}m_H nv\left(1 - \frac{2\phi kT}{mv}\right)Y(E)\,. \qquad (3)$$

Implicit in equation (3) is a summation over the atomic species in the gas.

2.3. *Vaporization*

Grain material is vaporized following a collision when the energy deposited by the shock wave propagating through the grain exceeds a certain threshold value. Once this threshold energy for vaporization is exceeded, the number of atoms vaporized from the target material will be approximately proportional to the collision kinetic energy. Studies of vaporization of silicate rocks and minerals which were conducted by colliding macroscopic rocks with a large slab of material at velocities of a few 10 km s^{-1} were summarized by Melosh (1989). These studies show that the onset of vaporization (incipient vaporization) in a gabbroic anorthosite (a typical lunar rock) occurs at pressures of (1.0–1.9) $\times$ 10^3 kbars (1 kbar = 10^9 dyn cm^{-2}), and complete vaporization starts at (5.9–7.9) $\times$ 10^3 kbars. In a planar approximation of these collisions, these pressures are exceeded at impact velocities of 7.5 km s^{-1} and 20 km s^{-1}, respectively, which correspond to kinetic energies of 6 and 42 eV per projectile atoms. Since the binding energy of this material is 6.7 eV, these studies suggest that the energies required to completely vaporize the solid must significantly exceed this value. Numerical simulations of hypervelocity collisions between gabbroic anorthosite projectiles onto gabbroic anorthosite surface (O'Keefe & Ahrens 1982) revealed that even at velocities of 25 km s^{-1} (65 eV per projectile atom), only traces of vapor were produced. At 30 km s^{-1}, the mass of the vapor produced increased sharply, reaching 3.5 times the projectile mass. Once the collision velocity exceeded 45 km s^{-1}, the simulations found that the vaporized mass $M_{\rm vap}$ is proportional to the collision kinetic energy and given by

$$M_{\rm vap} = 0.007\, M_P v_{\rm rel}^2\,, \qquad (4)$$

where M_P is the mass of the projectile, and $v_{\rm rel}$ is its velocity relative to the target material given in units of km s^{-1}. Equation (4) can be written as

$$N_{\rm vap} = \tfrac{1}{2}M_P v_{\rm rel}^2/E_{\rm vap}\,, \qquad (5)$$

where $N_{vap} = M_{vap}/\mathscr{A}m_H$ is the number of vaporized atoms, $\mathscr{A}$ is their mean atomic mass in atomic mass units, and m_H is the mass of the hydrogen atom. Equation (5) defines an effective binding energy $E_{vap} = 0.74\mathscr{A}$ eV, which for $\mathscr{A} = 20$, appropriate for gabbroic anorthosite, gives $E_{vap} = 15$ eV. Figure 21 in O'Keefe & Ahrens (1982) shows that the amount of vapor produced in the collision rises very sharply from its threshold velocity of 30 km s^{-1}, quickly approaching the asymptotic form given by equation (4). *The vaporization rate may thus be approximated by a step function, equal to zero below* $v_{rel} = 30$ km s^{-1}, *and given by equation* (4) *for higher velocities.* Generalizing the results of these simulations to collisions between objects with arbitrary masses M_T (the mass of the target material) and $M_P < M_T$, we write the equation for the amount of material vaporized in a collision as

$$N_{vap} = \begin{cases} 0 & v_{rel} \le 30 \text{ km s}^{-1}, \\ \frac{1}{2}\mu v_{rel}^2/E_{vap} & v_{rel} > 30 \text{ km s}^{-1}, \end{cases} \quad (6)$$

where $\mu = M_P M_T/(M_P + M_T)$ is the reduced mass of the system, and $E_{vap} = 15$ eV.

Equation (6) gives the total number of vaporized atoms N_{vap}, including both target and projectile grains. Note that above the threshold for vaporization, N_{vap} exceeds the number of atoms N_P in the projectile grain. In this case, the projectile grain is completely vaporized in the collision, while the target grain is generally only partially vaporized. The complete vaporization of the target grain occurs if the number of vaporized atoms calculated with the help of equation (6) is larger than the total number of atoms present in both target and projectile grains. Written in terms of velocities, the complete vaporization of the target grain takes place if the relative velocity v_{rel} exceeds the critical velocity v_{vap},

$$v_{vap} = \max \{30 \text{ km s}^{-1}, [2(N_T + N_P)E_{vap}/\mu]^{1/2}\}, \quad (7)$$

where N_P and N_T denote the number of atoms in the projectile and target grains, respectively.

Note that the concept of the effective binding energy E_{vap} in equations (6) and (7) has a meaning only for fast ($v_{rel} > 30$ km s^{-1}) collisions. No significant vaporization occurs in lower velocity collisions, even if the kinetic energy per atom exceeds E_{vap}. For example, according to our criteria a silicate projectile dust grain is not vaporized if it collides with the target grain with the relative velocity just below 30 km s^{-1}, although the collision kinetic energy per projectile atom exceeds 90 eV.

Our vaporization criteria are based on numerical calculations by O'Keefe & Ahrens (1982) and involve extrapolation to collision velocities higher than considered by these authors. A question arises as to how reliable these calculations are and whether extrapolation according to equation (4) is valid for velocities in excess of 100 km s^{-1}. A recent thorough analysis of grain vaporization in g-g collisions by Tielens et al. (1994) is in good agreement with the O'Keefe & Ahrens calculations, confirming the validity of equation (4) in the velocity range considered by these authors. Tielens et al. (1994) also find an approximate agreement between their analytical value of the velocity threshold for vaporization, equal to 16 km s^{-1}, and the threshold derived from these numerical calculations. As mentioned above, the numerical calculations actually suggest a somewhat higher value of 30 km s^{-1}.

The linear scaling of the vaporized mass on the projectile kinetic energy in equation (4) is only an approximation valid over a limited energy and velocity range. The reason is the same as for macroscopic cratering processes; the reader is referred to a review by Holsapple (1993) for an in-depth discussion of a scaling analysis in this context. The approximate nature of equation (4) is demonstrated by Tielens et al. (1994), who discuss grain vaporization using a theory of blast-wave propagation into a solid. An inspection of their Figure 8*a* shows that equation (4) is a reasonable (better than 30%) approximation for g-g collisions with velocities not exceeding 200 km s^{-1}. For still higher velocities, more accurate formulae given by Tielens et al. (1994) should be used. Because we do not consider such high-velocity grains in this work, we use an approximate equation (4) hereafter. Note that similar constraints apply as well to our criteria for catastrophic fragmentation and cratering, which are discussed next.

2.4. *Catastrophic Fragmentation*

A grain will fragment catastrophically if the collision energy exceeds a critical threshold value. We define the critical specific energy E_d (eV atom^{-1}) for grain destruction (rupture energy) as the collision kinetic energy per one atom of the target grain at the threshold for catastrophic fragmentation. We expect E_d to be approximately equal to $\mathscr{A}m_H\mathscr{T}/\rho$, where $\mathscr{T}$ (dyne cm^{-2}) is the tensile strength of the target material, ρ is its density, and $\mathscr{A}$ denotes the mean atomic mass in atomic mass units. The tensile strength depends in general on how the stresses are generated within the solid material. If the forces are applied slowly, then once they exceed the static tensile strength of the material, they will open the weakest crack. This crack will propagate through the grain leading to its fracture. The static tensile strength $\mathscr{T}_s$ depends on the density and the size distribution of flaws in the object. As a result, large objects will tend to be the weakest since statistically, they are more likely to have the largest flaws. Small grains are therefore expected to be relatively strong. In order to estimate their strength, consider a single crack in an otherwise flawless crystal lattice. This crack will open if the solid is subjected to a stress exceeding a critical value. This critical stress σ is a function of the crack length l:

$$\sigma = K_{IC}(\pi l)^{-1/2}, \quad (8)$$

where the fracture toughness K_{IC} depends on the solid structure. (In eq. [8], σ is measured far away from the crack; stresses near the crack are position dependent and exceed σ near the crack tips). For typical brittle materials, $K_{IC} = 100$ bars cm$^{1/2} = 10^8$ dyn cm^{-2} cm$^{1/2}$, so for a crack of length $l = 0.1$ μm the stress σ must exceed 20 kbars (2×10^{10} dyn cm^{-2}) for a break to occur. (These values of l and σ are appropriate for the largest interstellar grains; obviously, l must be smaller and σ higher for grains with radii less than 0.1 μm.) If we now equate this critical stress σ to the static tensile strength of a grain, we arrive at $\mathscr{T}_s = 2 \times 10^{10}$ dyn cm^{-2}. This value is orders of magnitude higher than for macroscopic bodies such as rocks, conglomerates, comets, or asteroids, the difference being primarily a result of the size dependence in equation (8).

Collisions between grains are dynamic processes in which forces are applied rapidly to the material, and the growth of cracks is not just limited to the weakest flaw (largest crack). As a result, many cracks can grow during the collision process, leading to the catastrophic fragmentation of the grain once the collision energy exceeds the dynamic tensile strength of the material. The dynamic tensile strength can be much larger than the static one; for example, in rocks it can exceed the static tensile strength by 1 order of magnitude. Using our estimate

for the grain static tensile strength, that suggests that the dynamic tensile strengths are in excess of 100 kbars (10^{11} dyn cm^{-2}). But this value is comparable to the ideal material strength. The required pressures to fragment a dust grain are so high that even ideal grains without any preexisting flaws can be fragmented. The fragmentation of grains is therefore quantitatively quite different from the breakup of macroscopic objects like asteroids which proceed at low pressures.

Consider a dynamical tensile strength of 100 kbars (10^{11} dyn cm^{-2}). For silicates with a density of $\rho = 3$ g cm^{-3} and $\mathscr{A} = 20$, this corresponds to E_d of 0.7 eV. Because the binding energy of a silicate atom is 6.7 eV, catastrophic fragmentation can therefore proceed when collision energies are about an order of magnitude smaller than the binding energy of the dust. Energies required for the complete vaporization of the grain are about 15 eV, so that in low-velocity shocks, the evolution of the grain size distribution is primarily controlled by the fragmentation of the dust and not their vaporization. Adopting a critical energy E_d for the catastrophic fragmentation of the dust that is equal to 0.1 $E_{\rm bind}$, we find that the threshold velocity for catastrophic collision can be written, in a similar fashion to the criteria for complete vaporization (eq. [7]), as

$$v_{\rm thr} = [2(N_T + N_P)E_d/\mu]^{1/2} , \quad (9)$$

where as in equation (7), N_T and N_P are, respectively, the number of atoms in the target and projectile grain, and μ is the reduced mass of the system. A target grain will fragment if the relative velocity of the collision exceeds the threshold velocity given in equation (9) above. (Note that this velocity may be much lower than the threshold velocity of 30 km s^{-1} for the vaporization to occur. For such low velocities, fragmentation and cratering are the only processes modifying the grain size distribution. This regime is not relevant in our present context but might be important in other physical situations.)

While we take $E_d = 0.1$ $E_{\rm bind}$ to describe the catastrophic fragmentation of the interstellar dust grains, the reader should be aware that E_d actually increases with the decreasing grain size. Smaller grains are expected to be stronger than larger grains, and more energy per each grain atom is needed to break them apart. This is explicitly demonstrated by recent experimental data and molecular dynamics simulations of the fragmentation of the molecular-sized carbon cluster C_{60} (Campbell et al. 1993; Schulte 1995). Approximately 4 eV of kinetic energy per each carbon atom must be involved in the collision in order to disrupt the cluster, several times as much as suggested by our criterion for E_d. This does not contradict our estimates for much larger grains of interest in this work, but it clearly shows that E_d increases with the decreasing grain size. By assuming constant $E_d = 0.1$ $E_{\rm bind}$, we have chosen to describe the strength of the interstellar dust grains in terms of a mean grain strength, averaged over the grain size distribution.

The size and velocity distribution of fragments produced in grain-grain collisions depend on the details of the shock propagation within grains. Experimental data in the parameter range of interest to grain-grain collisions are lacking, and any theoretical investigations are likely to be difficult and involve poorly known physical properties of interstellar dust grains. In view of these difficulties, we restrict ourselves to parameterizing the fragment size distribution in terms of universal power laws which have been found to hold in a variety of physical situations.

The size and velocity distribution of fragments can be described by the conditional probability $f(m, v \mid \mu, u, \mu', u')dmdv$ that particles with masses between m and $m + dm$ and velocities between v and $v + dv$ are formed in the breakup of a grain with mass μ and velocity u in a collision with a grain with mass μ' and velocity u'. We will assume that the fragmentation function f does not depend explicitly on the velocities of the target and the projectile grain or on the projectile mass μ'. However, we allow for the partial vaporization of the target grain, which does depend on these quantities. We denote the vaporized mass fraction of the target grain by r. The mass fraction deposited into fragments is then equal to $s = 1 - r$. We assume a simple and common power-law distribution $f \propto m^{-(x+1)}$ for these fragments. (For example, fragmented rocks obey this power law; Hartmann 1969). With these assumptions, f integrated over velocities can be written as (Hellyer 1970, 1971)

$$f(m \mid \mu, u, \mu', u') = (1 - x)s^x \frac{\mu^x}{m^{x+1}} , \quad (10)$$

with $\int fmdm = s\mu$ the total mass of the fragments. Note that equation (10) implies that there is a small but finite probability that the mass of the largest fragment is only a little less than $s\mu$. The parameter x in equation (10) was found to be in the range of 0.5–1 from experiments on rock fragmentation (Hartmann 1969). The actual distribution of fragments is more complicated, as reviewed recently by Fujiwara et al. (1989), but it still may be described by power laws in different ranges of fragment sizes. A recent theoretical study by Melosh, Ryan, & Asphaug (1992) accounts for these features of the fragment size distribution. However, these experimental and theoretical results cannot be easily extrapolated to microscopic grains of interest in this work. Likewise, it is hard to extrapolate very recent results on the fragmentation of the molecular-sized carbon cluster C_{60} to 0.01–1 μm grains. Both experiment and theory (Schulte 1995) show a power-law distribution of fragments at small fragment sizes and a more complicated distribution for large fragments, a situation analogous to that encountered in rock fragmentation. It is remarkable that these studies indicate that the power-law index x of the fragment size distribution for such a small cluster is only slightly smaller than that derived from experiments on rock fragmentation. This supports our use of equation (10) for the fragmentation of the interstellar dust grains. We note that parameter x is related to the power-law index p of the grain size distribution through relation $x = [(p + 2)/3] - 1$. For $p = 3.5$, the Mathis, Rumpl, & Nordsieck (1977, hereafter MRN) grain size distribution, x is equal to 0.833; this value of x is of particular interest.

While the velocity distribution of fragmentation products is not known, we expect that the mean fragment velocity is much smaller than the initial impact velocity. Note that this statement holds in the frame of reference at rest with respect to the target grain, or more precisely in the center of mass of colliding grains. For simplicity, we will assume that fragments are stationary in the center of mass of the colliding grains.

2.5. *Cratering*

Above a certain energy threshold, collisions with small grains can excavate a crater in a larger (target) grain. In this work, we are interested in the amount of material ejected from a crater and in the distribution of fragment sizes. For macroscopic craters, it is possible to estimate the crater size and the amount of ejected matter using a scaling analysis (see Holsapple 1993 for a recent review). This scaling analysis presumes the knowledge of physical processes relevant for the fragmentation

and the excavation flow leading to the crater formation. Again, while relevant physical processes have been studied extensively in the context of macroscopic hypervelocity collisions, little is known about microscopic cratering events of interest in this work. Quantities such as the material strength, the kinetic energy and momentum of the projectile grain, and viscosity in the excavation flow are likely to be important. There have been only a few experimental studies on microcraters with diameters of interest here, less than 0.1 μm. Katakuse et al. (1992) studied formation of nanometer-sized craters by bombarding graphite with CsI clusters. They found that the crater diameter depends primarily on the cluster energy, and not on its mass and momentum. This is in agreement with the results obtained for macroscopic craters, in which the projectile kinetic energy was found to be the most important parameter determining the crater size. This can be understood by noting that the well-known solutions for a propagation of a strong blast wave in a uniform medium do indeed scale with the explosion energy. The evolution of the hemispherical shock wave propagating from the impact site can be modeled to the first order by these spherically symmetric solutions. Katakuse et al. (1992) observed nanometer-sized (6 nm in diameter) craters upon bombardment of the graphite surface with $\sim$180 atom CsI clusters with velocity of 15 km s^{-1} and energy 30 keV. The observed crater site implies removal of $\sim$6000 carbon atoms from the impact site, requiring an expenditure of $E_{cr} = 4.7$ eV atom^{-1}. Note that this value is larger than the mean energy per atom required for catastrophic fragmentation of the grain but less than the value needed for grain vaporization. The exact number is, of course, uncertain. For example, the CsI clusters in experiments done by Katakuse et al. (1992) are quite large, 2.5 nm in diameter, and comparable to the observed crater sizes. Therefore, it is likely that in these experiments the crater size depends sensitively on events occurring right after the impact. A proper understanding of this early postimpact phase requires molecular dynamics simulations in view of the small ($\sim$180 atoms) sizes of CsI clusters (Cleveland & Landman 1992). This makes an extrapolation to higher energies and velocities of interest to us uncertain.

The destruction of grains by cratering can be regarded as a slow and continuous erosion process, not unlike sputtering. Therefore, we will express the grain erosion rate by cratering collisions in a form similar to the rate of grain erosion by kinetic sputtering, with small projectile grains assuming the role of incident gas atoms, and the ejected fine dust assuming the role of the atoms (molecules) that are sputtered from the grain surface. We will refer to these projectile grains as stationary (field) grains, because the case of most interest involves a dust grain moving with respect to the dusty ambient (stationary) medium. The erosion rate due to cratering collisions by dust particles of mass m_f and number density $n(m_f)$ impinging on the target grain of mass m and radius a with a relative velocity v can then be written as

$$\dot{m}_{cr} = -\mathscr{A} m_H n(m_f) \pi a^2 v Y_{cr} = -n(m_f) \pi a^2 v f_c m , \quad (11)$$

where $\mathscr{A}$ is the mean atomic mass in amu of a constituent atom in the fine dust, and Y_{cr} is a dimensionless cratering yield taken to be equal to $m_f v^2/2E_{cr}$, where E_{cr} is the specific energy (eV atom^{-1}) for the ejection of one atom in a cratering event. The product $\mathscr{A} m_H Y_{cr}$ defines the average mass excavated in each collision, which can be written as $f_c m$, where f_c is the fraction of the mass m of the target grain that is ejected from the crater. Since the ejected atoms are clustered together forming a large number of fragments, E_{cr} is expected to be less than the dust binding energy, E_{bind}, but larger than the critical energy for grain destruction, E_d. For convenience, we will adopt the geometric mean of E_d and E_{bind} as the standard value for E_{cr}, i.e., $E_{cr} = (E_d E_{bind})^{1/2}$. Note that the difference in the specific energies between catastrophic and cratering collisions reflects our previous comments about the relative strength of small and large grains; given the same amount of available energy per atom in the whole grain or in the crater, it should be easier to disrupt the whole grain than to eject a proportionally high amount of material from a much smaller crater. The reader should also realize that the two discrete quantities E_d and E_{cr} merely serve as a convenient parameterization of the continuous distribution of the grain strength as a function of size; on average, craters are much smaller than whole grains undergoing catastrophic collisions. Adopting a maximum value of f_c, beyond which cratering collisions will be regarded as catastrophic collisions, we can calculate the erosion rate of a given grain of mass m resulting from collisions with all dust particles that produce craters with a mass less than $f_c m$. The mass of these field grains must be less than $2E_{cr} f_c m/\mathscr{A} m_H v^2$. The total erosion rate of a given grain is obtained by integrating equation (11) over all impinging dust particles with masses $\leq m$.

For an extended MRN grain size distribution with the maximum grain size a_{max}, extending down to very small dust grains with the power-law index p, the spatial mass density $\rho_d(<m_f)$ of dust grains with masses less than m_f is equal to $(a_f/a_{max})^{4-p}\rho_d$ (for $p < 4$), where $\rho_d = Z_d \rho$ is the total spatial mass density of dust, ρ is the mass density of the gas, and Z_d is the dust-to-gas mass ratio. Then we can write the erosion rate of a grain of radius a, resulting from collisions with a population of test grains with an a^{-p} distribution in grain sizes, as

$$\dot{m}_{cr} = -\frac{Z_d \rho \mathscr{A} m_H \pi a^2 v^3}{2E_{cr}} \left(\frac{a_f}{a_{max}}\right)^{4-p} , \quad (12)$$

with a_f defined as

$$\frac{a_f}{a} \equiv \left(\frac{2E_{cr} f_c}{\mathscr{A} m_H v^2}\right)^{1/3} . \quad (13)$$

There is some ambiguity as to which impacts should be considered as cratering events because of a somewhat artificial distinction between the catastrophic fragmentation and the formation of a crater comparable in size to the target grain. For example, approximately 15% of the target grain mass would be ejected from a crater with radius equal to two-thirds of the target grain radius. Such collision would not lead to the catastrophic fragmentation according to our criteria discussed in § 2.4, but it can hardly be classified simply as an eroding event. In principle, this dilemma can be resolved successfully with a suitable definition of the fragmentation function f (§ 2.4). However, in view of considerable uncertainties in our understanding of the fragmentation and cratering processes, we did not attempt to resolve this problem, and instead of constructing a self-consistent, elaborate scheme to distinguish between such collisions, we chose a practical alternative and assumed that collisions which eject less than 10% of the target grain mass are cratering events. The grain erosion rate is then calculated by taking into account only such collisions, which is equivalent to setting $f_c = 0.1$ in equation (12). Because of poorly known thresholds for cratering and fragmentation, we consider such an approximate algorithm adequate for our purposes, particularly in view of a weak dependence of the erosion rate $\dot{m}_{cr}$ on f_c (eqs. [12] and [13]).

As a result of the cratering process, a larger number of small fragments is ejected from craters. In order to find their size distribution in the present case, for the power-law distribution of field grains, we assume that in each cratering event fragment sizes are also described by a power-law distribution with the same index p. Then we find that a fraction of the total fragment mass contained in fragments with dimensionless radii less than a_{fr} is equal to $a_{fr}^{4-p}(1 - \ln a_{fr}^{4-p})$. Here fragment radii are measured relative to the radius of the largest fragment produced in all cratering collisions. (Note that the mass of the biggest fragment must be smaller than the maximum mass removed from a crater, equal to 10% of the target grain mass for $f_c = 0.1$.) This result differs from the power-law distribution by the presence of the logarithmic term. This extra term makes the distribution much steeper, with a strong excess of small over large grains as compared to the initial power-law distribution. For example, consider a 0.25 μm grain slowing down in a dusty medium. The largest fragment size ejected from any cratering event cannot by definition exceed 0.1 μm. If fragment sizes were distributed according to the extended MRN distribution with $p = 3.5$, one-half the total fragment mass would be contained in grains larger than 0.025 μm. But because of the presence of the logarithmic term, only 15% of mass is contained in such large grains, and more than 50% is deposited in very small (<0.004 μm) fragments (we took $p = 3.5$ for these estimates).

3. DESTRUCTION OF DUST GRAINS

3.1. *Grain Erosion by Sputtering and Cratering*

A dust grain moving through the ambient gas is decelerated in collisions with atoms and ions within the gas. This deceleration is given by

$$\frac{dv}{dt} = -\frac{\beta\pi a^2 \rho v^2}{m}, \tag{14}$$

where v is the grain velocity, m and a are its mass and radius, ρ denotes the gas density, and β is the enhancement of the collisional drag in a plasma relative to that in a neutral medium. This enhancement is substantial in ionized gases (Shull 1978; Draine & Salpeter 1979a), where β is a function of the grain velocity and may be much larger than unity. In this work, we are concentrating our efforts on grains moving at high speeds through neutral gas, where $\beta = 1$. This situation is relevant for radiation pressure–accelerated dust grains in red giant winds, and for those grains in shock waves which penetrated into the cold and neutral postshock region. We took $\beta = 1$ in most calculations presented in this paper; our numerical results are valid only for the neutral gas. The reader should be aware that grain destruction decreases with increasing β as can be deduced from our discussion below. In particular, this will affect small dust grains moving through ionized gas. (Note also that β may be somewhat different from unity for low grain velocities, comparable with the mean thermal velocity of the gas; Baines, Williams, & Asebiomo 1965.)

A decelerating grain also undergoes collisions with stationary (field) grains, which results in grain erosion through cratering or in a complete disruption of the grain as discussed above. The latter process either completely vaporizes the grain or redistributes its mass into a large number of fragments, while erosion leads to a gradual decrease in grain radius and mass. Excluding catastrophic events, any grain can be regarded as moving in its mass-velocity $\{m, v\}$ space, from an origin given by its initial mass and velocity. The trajectory may terminate either "peacefully" as the grain decelerates and joins the population of stationary field particles, or catastrophically, when it completely vaporizes or fragments at a given point along the trajectory. The decrease in grain mass along its trajectory is given by

$$\frac{dm}{dt} = \dot{m}_s + \dot{m}_{cr}, \tag{15}$$

or

$$\frac{dm}{dv} = -\frac{m(\dot{m}_s + \dot{m}_{cr})}{\beta\pi a^2 \rho v^2}, \tag{16}$$

where the sputtering and the cratering rates, $\dot{m}_s$ and $\dot{m}_{cr}$, are given by equations (3) and (12), respectively. Equations (14) and (15), or equation (16), together with the initial grain mass and velocity, determine the grain motion in $\{m, v\}$ space.

We will define a dimensionless quantity, $d\ln m/d\ln v$, that measures the relative importance of grain erosion and deceleration. From equation (16) we obtain

$$\frac{d\ln m}{d\ln v} = -\frac{(\dot{m}_s + \dot{m}_{cr})}{\beta\pi a^2 \rho v} = 0.935\left(1 + \frac{\dot{m}_s}{\dot{m}_{cr}}\right)\left(\frac{Z_d}{0.0075}\right)\left(\frac{\beta}{1.0}\right)^{-1}\left(\frac{f_c}{0.1}\right)^{1/6} \times \left(\frac{v}{100\ \mathrm{km\ s^{-1}}}\right)^{5/3}\left(\frac{E_{cr}}{2\ \mathrm{eV}}\right)^{-5/6}\left(\frac{a}{a_{max}}\right)^{4-p}. \tag{17}$$

In Figure 2, we plot $d\ln m/d\ln v$ as a function of grain velocity for two very different grain radii, 0.02 and 0.25 μm, with a cratering threshold $E_{cr} = 2$ eV, $f_c = 0.1$, and decelerating in neutral gas ($\beta = 1$). The stationary dust particles are characterized by an MRN dust grain size distribution with $a_{max} = 0.25$ μm, extended to small grain sizes and a standard dust-to-gas mass ratio $Z_d = 0.0075$. These are our standard model parameters, which we list in Table 1 for future reference. Because $d\ln m/d\ln v$ is of order of unity for velocities and grain radii of interest, the grain erosion is substantial, particularly for large, fast-moving grains. Both cratering and sputtering are important, as can be seen in Figure 2. In Figure 3 we present the sputtering/cratering rate ratio, $\dot{m}_s/\dot{m}_{cr}$, as a function of grain velocity for a number of grain radii. The curves show that at velocities above ~ 70 km s^{-1} the sputtering to cratering rate ratio is roughly constant, independent of grain velocity. (Analysis of its dependence on modal parameters shows that it scales linearly with E_{cr} and inversely with Z_d.) This results from the fact that above this velocity both the sputtering and the cratering yields increase linearly with energy in the velocity range considered in the figure. At velocities below ~ 70 km s^{-1}, the ratio falls rapidly as the sputtering threshold is approached. Since, by definition, cratering occurs by collisions of the fast-moving grain with smaller size field particle, the relative importance of cratering increases with grain size, as $a^{-(4-p)} = a^{-1/2}$ for $p = 3.5$ (MRN distribution); see equations (12) and (13). The larger the fast-moving grain, the more it encounters smaller stationary grains that exceed the cratering threshold. This is in contrast with sputtering, where the sputtering rate per unit area is independent of grain size.

For grains moving through a homogeneous ambient medium, the right-hand side of equation (17) does not depend on time t. The grain mass is then a function of its velocity v alone and can be found by solving equation (17). The grain trajectory $m(v)$ in $\{m, v\}$ space is completely determined by the combined effects of sputtering, cratering, and the collisional drag. Consider fast grains with velocities larger than 70–80 km s^{-1} so that $\dot{m}_s/\dot{m}_{cr}$ may be assumed to be independent of the

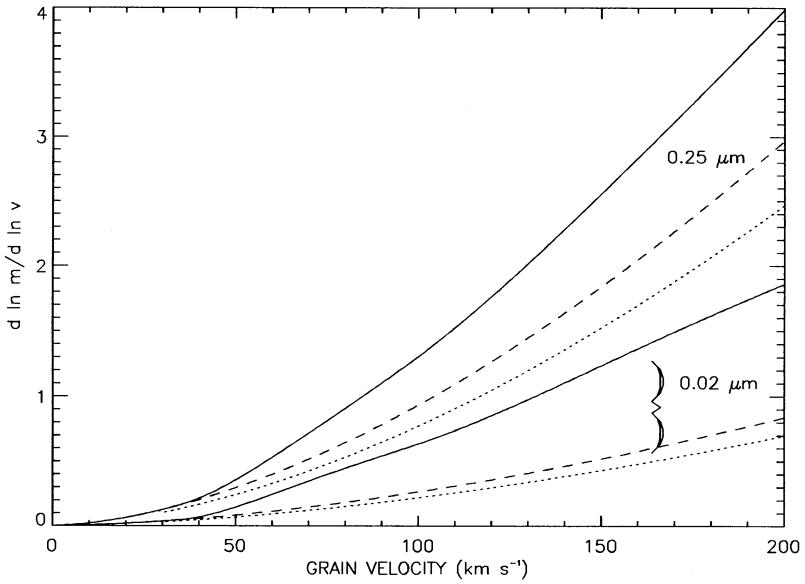

FIG. 2.—Ratio $d \ln m/d \ln v$ (eq. [17]) is shown as a function of grain velocity v and grain radius a. Solid curves depict the ratio for grain erosion as a result of combined effects of cratering and sputtering, and dashed curves are for the case when grains are eroded as a result of cratering alone. Dotted curves show the production rate of fine dust particles in cratering events, which is less than the cratering rate because of the partial vaporization of the grain material in the cratering process. Model parameters used for the calculations are described in the text (§ 3.1).

grain velocity v (Fig. 3). This sputtering/cratering rate ratio depends then on the grain size alone. If β is constant, equation (17) can be solved analytically to give the grain mass as a function of velocity

$$m(v) = m_0 \left[\frac{\alpha_0}{(1 + \alpha_0) \exp \{0.1 R_0 \alpha_0 [1 - (v/v_0)^{5/3}]\} - 1} \right]^6 \qquad v > 70 \text{ km s}^{-1}, \quad (18)$$

for the grain trajectory passing through m_0 and v_0. The parameter R_0 is defined as the logarithmic ratio of cratering and deceleration rates (eq. [17] with $\dot{m}_s$ set to zero), evaluated at $a = a_0$ and $v = v_0$, while α_0 is the sputtering/cratering rate ratio $\dot{m}_s/\dot{m}_{cr}$ also evaluated at a_0 and v_0.

At velocities below the sputtering threshold, less than 50 km s^{-1}, $\dot{m}_s$ can be set to zero in equation (17). If β is constant, equation (17) can be also solved analytically to give

$$m(v) = m_0 \{0.1 R_0 [1 - (v/v_0)^{5/3}] + 1\}^{-6} \qquad v < 50 \text{ km s}^{-1}, \quad (19)$$

for the grain trajectory passing through m_0 and v_0.

Figure 4 shows representative grain trajectories in $\{a, v\}$ space. These trajectories were calculated numerically with the help of equation (17) and for the standard model parameters. The trajectories can be accurately represented by

$$a(v) = \left[\frac{0.227}{(1 + 0.227 a_{100}^{-1/2}) \exp \{0.0467 [1 - (v/100 \text{ km s}^{-1})^{5/3}]\} - 1} \right]^2 \quad (20)$$

for 50 km s^{-1} $< v <$ 200 km s^{-1}, and by

$$a(v) = \frac{a_{50}}{\{0.0589 a_{50}^{1/2} [1 - (v/50 \text{ km s}^{-1})^{5/3}] + 1\}^2} \quad (21)$$

for $v <$ 50 km s^{-1}, where a_{50} and a_{100} are the points on the trajectory that correspond to the grain radius (μm) at velocities of 50 km s^{-1} and 100 km s^{-1}, respectively.

The figure shows that the erosion of large, fast-moving grains is substantial because of high cratering and sputtering rates. For example, a 0.25 μm grain injected with velocity of 200 km s^{-1} into ambient gas comes to rest with its final radius of only 0.11 μm (Fig. 4). This means that 91% of its original

TABLE 1

STANDARD MODEL PARAMETERS

Parameter	Abbreviation	Value
Ambient Medium		
Dust-to-gas mass ratio	Z_d	0.0075
Deceleration parameter	β	1.0
Power-law index of the initial grain size distribution	p	3.5
Maximum grain radius	a_{max}	0.25 μm
Collision Parameter		
Cratering threshold	E_{cr}	2 eV
Critical rupture energy	E_d	0.67 eV
Effective binding energy	E_{vap}	15 eV
Threshold velocity for vaporization	...	30 km s^{-1}
Maximum excavated mass fraction in cratering collisions	f_c	0.1
Power-law index of the fragment size distribution	p	3.5

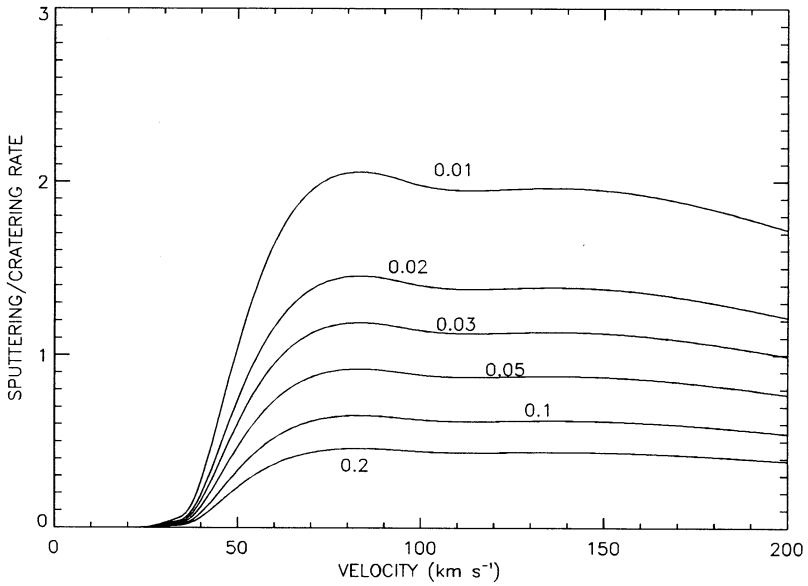

FIG. 3.—The ratio of the sputtering rate to the cratering rate as a function of grain velocity. Curves are labeled by the grain radius a (μm). Model parameters are identical to those used in Fig. 2.

mass was lost by either sputtering or cratering, before the grain had decelerated, and only 9% of its mass is contained in the surviving grain. For all practical reasons, large, fast-moving grains are efficiently destroyed by cratering and sputtering. This point is further illustrated in Figures 5 and 6, in which we plot separately the mass fraction removed from grains by cratering and sputtering, respectively. For a 0.25 μm grain with the initial velocity of 200 km s^{-1}, 56% of grain mass is removed by cratering and 35% by sputtering. Both rates are steep functions of grain velocity, with cratering being more important than sputtering for large initial grain sizes. The opposite is true for small grains: cratering becomes negligible in comparison with sputtering.

As discussed in § 2.5, the grain material is ejected from craters in the form of tiny dust particles, with velocities much smaller than the grain velocity v in the frame of reference comoving with the grain. They can then be considered stationary with respect to the grain, but not with respect to the ambient gas or dust. They are effectively injected into gas with the velocity of the grain at the time of impact. Because of their small sizes, they are quickly decelerated in collisions with electrons, atoms, and ions. However, if v is sufficiently large, a significant amount of grain material can be sputtered during this deceleration process. Therefore, the total sputtered mass depicted in Figure 6 includes not only direct sputtering from a decelerating grain, as given by $\dot{m}_s$ in equation (17), but also sputtering of fragments ejected from craters. The sputtered mass fraction is almost independent of the grain size in the limit of small grain radii where cratering is not important; we plot this fraction in Figure 6 for a dust particle 0.002 μm in

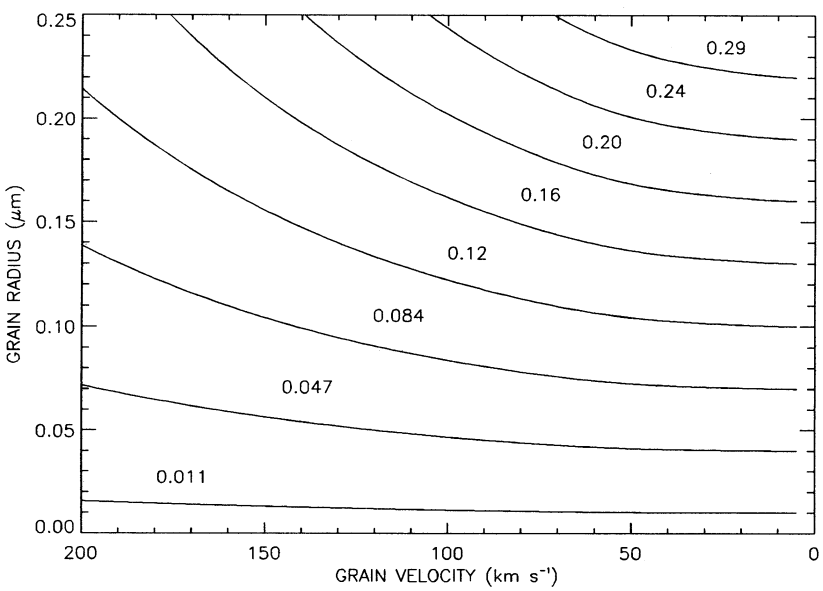

FIG. 4.—Grain trajectories in the grain radius–velocity space, for standard model parameters. The trajectories depict the evolution of particles with any initial radius a_0 and velocity v_0 in $\{a, v\}$ space, starting from an initial location at $\{a_0, v_0\}$. Each trajectory is labeled by its value of a_{100}, grain radius in μm at 100 km s^{-1}.

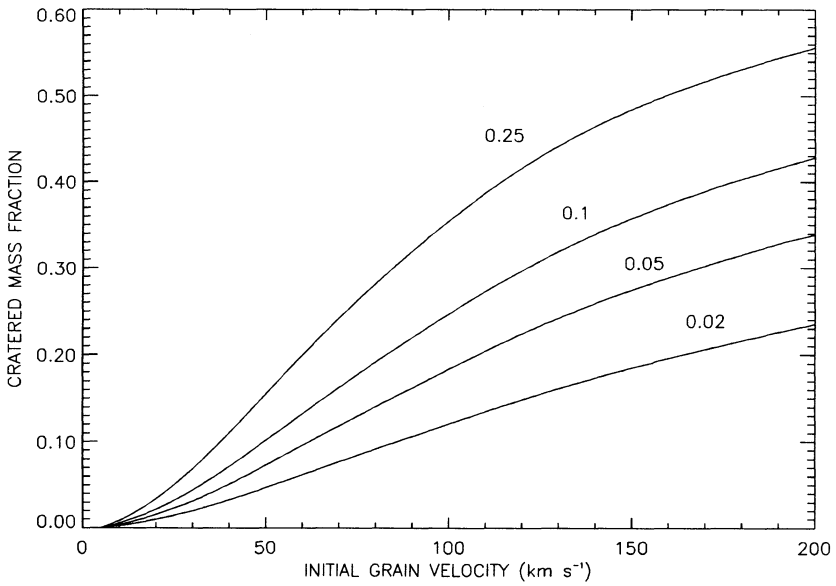

FIG. 5.—Mass fraction removed from grains by cratering vs. *initial* grain velocity. Curves are labeled by the *initial* grain radius (μm).

radius. Because of this invariance with respect to the grain size, the total sputtered mass fraction does not depend on the size distribution of fragments ejected from craters, and consequently it does not depend on the initial grain size. Similarly, after accounting for partial vaporization of grain material as described in § 3.3, we find that the total mass returned to the gas phase through vaporization and sputtering (shown in Fig. 6 by dashed curve, with sputtering dominating over vaporization) is also independent of the initial grain size.

Figure 7 shows the relative distribution between sputtered and vaporized grain mass, mass deposited in small particles, and the final grain mass, as a result of sputtering (including the sputtering of fragments ejected from craters) and partial vaporization of the grain material. As discussed above, the sputtered and vaporized mass fraction are independent of the initial grain radius and increase with the initial grain velocity. The mass fraction left in the surviving remnant of the grain does depend on the initial grain radius and is smaller for larger grains because cratering is efficient for large grain sizes. For a 0.25 μm grain with the initial velocity of 200 km s^{-1}, 60% of its mass is returned to gas through sputtering and vaporization, 31% is deposited into fine fragments, and only 9% is contained in the grain remnant, 0.11 μm in size. This partition does not take into account catastrophic fragmentations which will be discussed next. While catastrophic fragmentations reduce the number of surviving grains, the total mass fraction returned to the gas phase (shown in Fig. 7) should not be affected because of the invariance of the sputtered mass on the grain radius.

We have modeled cratering as a smooth process which continually erodes the grain, and which together with sputtering

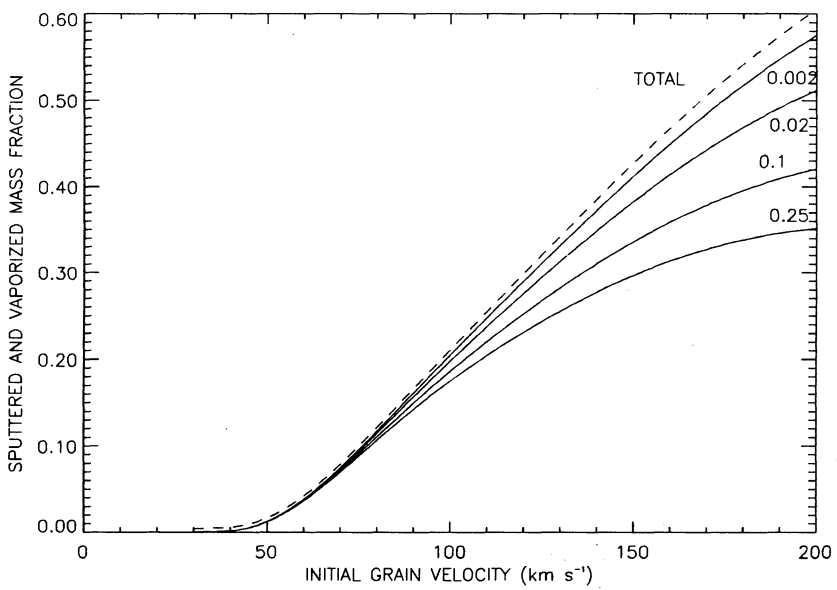

FIG. 6.—Mass fraction removed from grains by sputtering vs. *initial* grain velocity. Curves are labeled by the *initial* grain radius (μm). Dashed line is the sputtered mass fraction to which we have added both the mass sputtered from the fragments that were ejected in the cratering process and the mass vaporized from grains during cratering collisions. This mass fraction does not depend on the grain radius.

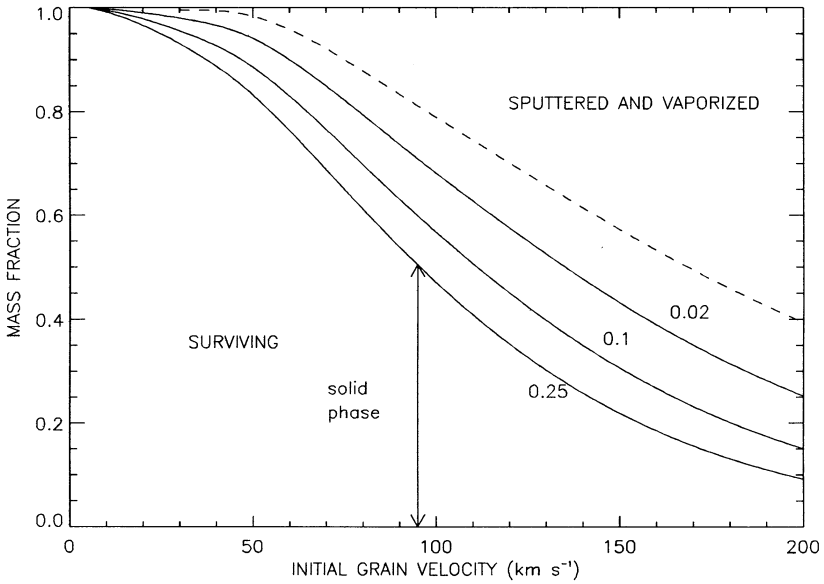

FIG. 7.—The relative distribution between sputtered and vaporized grain mass, mass deposited in small dust particles, and the final mass of the grain. The sputtered and vaporized mass fraction does not depend on the grain mass. Solid lines show the mass fraction contained in surviving grains, labeled by their *initial* grain radii (μm). The region between solid and dashed lines contains fine dust particles. Catastrophic fragmentation is not included.

and plasma drag determines its motion along the trajectories in $\{m, v\}$ space. While this appears to be a good approximation, cratering is a truly stochastic process, in which finite-sized craters are produced in collisions with field particles. Such collisions appear as discontinuities in the grain trajectory, where the grain jumps from one trajectory to another. In other words, grains not only move (drift) along their trajectories, but they also diffuse across these trajectories. The trajectories shown in Figure 4 should then be considered as mean trajectories, averaged over many grain paths. The diffusion across these mean trajectories is a second order effect which we neglected in this work. Before proceeding further, we just make a few statements about this diffusion.

The average mass excavated in cratering events, $\langle m_{cr} \rangle$, is equal to $\int m_{cr}^2 n(m_f) dm_f / \int m_{cr} n(m_f) dm_f$, where $n(m_f)$ is the distribution of field grains as a function of their mass m_f, m_{cr} is the mass ejected from the crater, and the integration is carried over all cratering collisions. For a power-law distribution of field grains with index p, $\langle m_{cr} \rangle$ is equal to $(4 - p)/(7 - p) f_c m$, where $f_c m$ is the maximum crater mass according to our discussion in § 2.5. Because this is a small fraction of the target grain mass, a description in terms of the mean erosion rate $\dot{m}$ and a fluctuating component $\sigma\xi(t)$ seems appropriate, so that the eroded mass is equal to $\dot{m}t + \sigma\xi(t)$. Here $\sigma\xi(t)$ is a Gaussian stochastic process with zero mean and variance $\sigma^2 t$. Stochastic process $\xi(t)$ is defined as a Gaussian process with zero mean and variance t, i.e., a standard Brownian motion, while σ^2 is given by

$$\sigma^2 = \frac{\langle m_{cr} \rangle \dot{m}}{1 + \dot{m}_s/\dot{m}_{cr}} = \frac{(4 - p) f_c m \dot{m}}{(7 - p)(1 + \dot{m}_s/\dot{m}_{cr})} . \quad (22)$$

The factor $1 + \dot{m}_s/\dot{m}_{cr}$ in the denominator of equation (22) accounts for the effects of sputtering, which does not produce appreciable diffusion. In order to study the diffusion effects, equation (15) should not only include the mean erosion rate $\dot{m}$ but also the fluctuating component $\sigma\xi(t)$. The resulting stochastic differential equations or an associated Fokker-Planck equation can be studied numerically. However, as was just mentioned, we neglect diffusion in this exploratory work.

3.2. *Grain Destruction by Catastrophic Fragmentation*

Dust grains are not only losing their mass through sputtering and cratering, but they can be destroyed by complete vaporization and catastrophic fragmentation as a result of grain-grain collisions. The destruction rate C (s^{-1}) of grains with mass m moving through ambient medium with velocity v, as a result of catastrophic fragmentation, can be written as

$$C(m, v) = \int_{m_{thr}}^{m_{max}} n_f(\mu') v \sigma(m, \mu') d\mu' , \quad (23)$$

where $n_f(u')d\mu'$ is the number density of stationary ("field") dust grains with masses between μ' and $\mu' + d\mu'$, $\sigma(m, \mu')$ is the geometrical cross section for grain-grain collision $\{= \pi[a(\mu') + a(m)]^2\}$, m_{thr} is the mass threshold for a disruptive collision at the velocity v, and m_{max} is the upper limit on the grain size distribution. At high velocities, where the mass threshold m_{thr} is much smaller than m, m_{thr} is simply equal to $2NE_d/v^2$ (N denotes the number of atoms in the target grain). At lower velocities, we use our criterion for the catastrophic fragmentation (eq. [9]) and find m_{thr} by setting $v_{thr} = v$ in this criterion.

For a power-law size distribution of field grains, the destruction rate C can be written as

$$C(m, v) = F(m, v) \pi a^2 v n_f(a_{thr}, a_{max}) , \quad (24)$$

where F is a factor of order of unity and $n_f(a_{thr}, a_{max})$ is the number density of field grains bigger than the velocity-dependent threshold size a_{thr} for catastrophic fragmentation. F is given by

$$F(m, v) = \left\{ 1 + \frac{2(p - 1) a_{max} [g^{(p-2)/3} (a_{max}/a)^{p-2} - 1]}{(p - 2) a [g^{(p-1)/3} (a_{max}/a)^{p-1} - 1]} + \frac{(p - 1) a_{max}^2 [g^{(p-3)/3} (a_{max}/a)^{p-3} - 1]}{(p - 3) a^2 [g^{(p-1)/3} (a_{max}/a)^{p-1} - 1]} \right\} , \quad (25)$$

with

$$g = 2[z - 2 - (z^2 - 4z)^{1/2}]^{-1} \quad (26)$$

and

$$z = \frac{\mathscr{A} m_H v^2}{2E_d}, \quad (27)$$

while

$$n_f(a_{thr}, a_{max}) = \frac{g^{(p-1)/3} n_f(a) a}{p-1} \times [1 - g^{-(p-1)/3}(a/a_{max})^{p-1}] . \quad (28)$$

The catastrophic fragmentation is comparable in importance to cratering. This can be seen in Figure 8, in which we plot $C(m, v)(d \ln v/dt)^{-1}$ for grain radii of 0.02 and 0.25 μm, for the standard model parameters.

Since catastrophic collisions are a noncontinuous grain destruction process, they can be best formulated in a statistical sense; that is, the way they attenuate a beam of dust particles moving through a distribution of stationary field particles. Consider then a beam of dust grains with an initial velocity v_0 and an initial mass m_0 that is injected into an ambient medium. The equation describing the evolution of n_b in a homogeneous medium is

$$\frac{dn_b}{dt} = -C(m, v) n_b , \quad (29)$$

where the grain mass m and its velocity v are evolving from their initial values m_0 and v_0 according to equations (14) and (15). It is convenient to define the function τ

$$\tau(v) \equiv -\int_0^v \frac{C(m, v)}{dv/dt} dv , \quad (30)$$

where the integration is carried along a trajectory in the grain $\{m, v\}$ space from the origin $\{m_0, v_0\}$ as depicted in Figure 4.

The solution of equation (29) is then

$$n_b = n_{b0} \exp [\tau(v) - \tau_0] , \quad (31)$$

where $n_{b0} = n_b(v_0)$ denotes the initial number density of dust grains and $\tau_0 \equiv \tau(v_0)$. The function τ can be interpreted as an "optical depth" for grain destruction, since the fraction of grains with an initial radius a_0, injected with the initial velocity v_0 into ambient medium, that escape any catastrophic collision is equal to exp $(-\tau_0)$, after they have completely decelerated and $\tau(v) \to 0$ for $v \to 0$. It is not surprising that the concept of optical depth is useful in the context of catastrophic g-g collisions; exactly the same probabilistic framework is widely used for a more familiar photon absorption. We plot τ_0 as a function of the initial grain velocity v_0 in Figure 9, for grains moving along the trajectories given by equations (20) and (21) (some of which are shown in Fig. 4), and with $E_d = 0.67$ eV. The optical depths shown in Figure 9 scale with the initial grain radius as $a_0^{0.47}$. The destruction rate is substantial, particularly for large, fast-moving grains. For example, $\tau_0 = 1.38$ for a grain with the initial radius of 0.25 μm and the initial velocity of 200 km s^{-1}. This means that only 25% of such grains will be able to decelerate intact, albeit eroded, with the remainder destroyed by catastrophic collisions.

The grain number density n_b changes with velocity according to equation (31), where τ is evaluated along the grain trajectory. In Figure 10, we plot optical depth τ along grain trajectories shown in Figure 4. Together with equation (31), these curves give solutions for n_b as a function of grain velocity, the initial grain radius a_0 and the initial velocity v_0.

3.3. *Partial and Complete Vaporization*

Vaporization of grain material in g-g collisions occurs in both cratering and catastrophic collisions. We have already implicitly taken vaporization into account in our calculations of the grain destruction rate C (eq. [23]), by including all collisions above the catastrophic fragmentation threshold. That includes completely vaporizing collisions. But in order to find

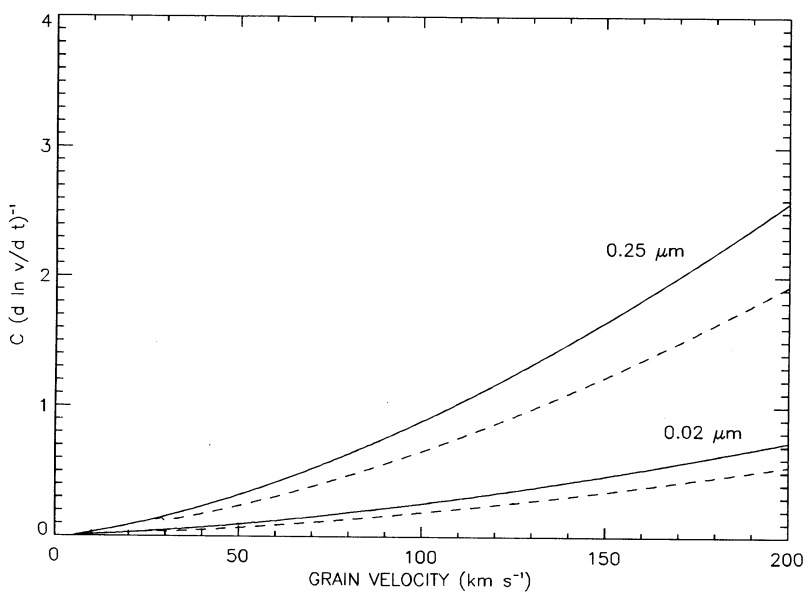

FIG. 8.—The dimensionless destruction rate $C(m, v)(d \ln v/dt)^{-1}$ as a function of grain velocity v and grain radius a. Solid lines depict the destruction rate by catastrophic fragmentations. Catastrophic fragmentation is comparable in importance to cratering (see Fig. 2). Dashed lines show the fragment production rate, which is less than the destruction rate because of complete and partial vaporization of the grain material in the collision process.

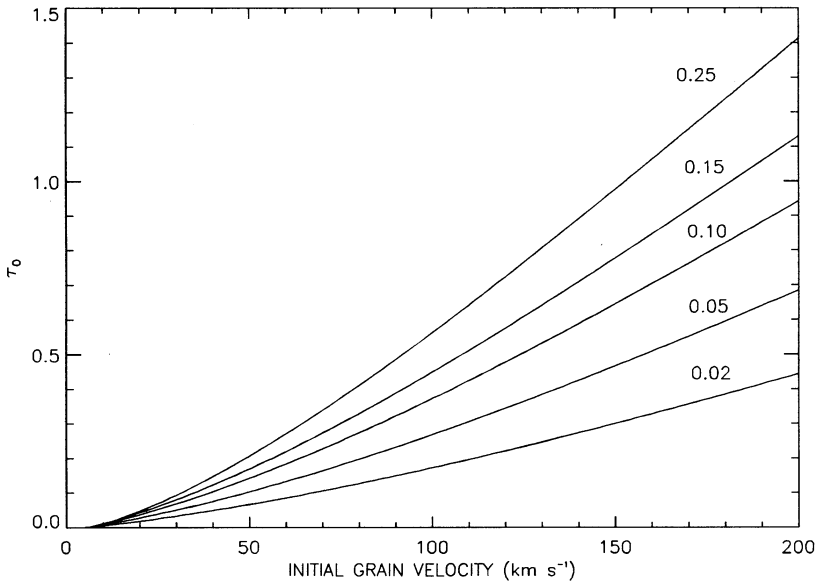

FIG. 9.—Optical depth τ_0 (see eqs. [29]–[30]) for grain destruction vs. *initial* grain velocity, for standard model parameters. Curves are labeled by the *initial* grain radii (μm).

the amount of material returned to the gaseous phase, or alternatively the fragment production rate, we need to estimate the partial and complete vaporization rate in g-g collisions.

The rate of completely vaporizing collisions, $C_c(m, v)$, can be found in the same fashion as the destruction rate C, with the help of equations (24)–(28). The only difference is that the critical rupture energy E_d in equation (27) is replaced by the effective binding energy $E_{\rm vap}$. According to our discussion in § 2.3, vaporizing collisions occur only for velocities in excess of 30 km s^{-1}. Above this velocity threshold, the fraction of completely vaporizing collisions is approximately constant, with $C_c/C \approx 11\%$–13%.

Partial vaporization appears to be somewhat more effective than complete vaporization. According to equation (6), an effective destruction rate for partially vaporizing collisions, $C_p(m, v)$, for a grain with mass m moving with velocity v through the ambient medium, can be written as

$$C_p(m, v) = \int_0^{m_{\rm vap}} \frac{\mu v^2}{2E_{\rm vap} N} n_f(\mu') v \sigma(m, \mu') d\mu' , \qquad (32)$$

where N is the number of grain atoms, $\mu = m\mu'/(m + \mu')$ denotes the reduced mass, and $m_{\rm vap}$ denotes the mass threshold for completely vaporizing collisions. Again, at high velocities, where the mass threshold $m_{\rm vap}$ is much smaller than m, $m_{\rm vap}$ is simply equal to $2NE_{\rm vap}/v^2$. At lower velocities, we use our criterion for the completely vaporizing collisions (eq. [7]) and find $m_{\rm vap}$ by setting $v_{\rm vap} = v$ in this criterion. For a power-law

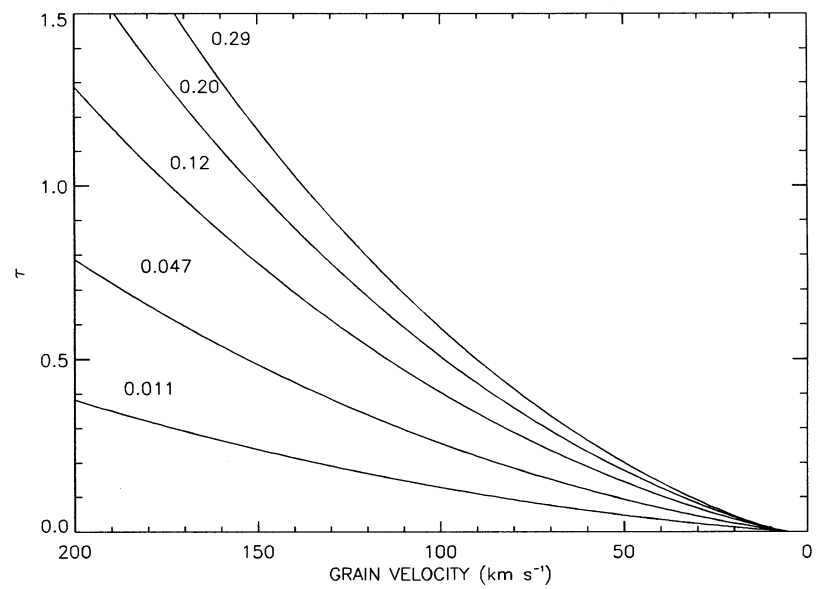

FIG. 10.—Optical depth τ for grain destruction along the trajectories shown in Fig. 4. Each trajectory is labeled by its value of a_{100}, grain radius in μm at 100 km s^{-1}.

size distribution of field grains, C_p can be written as

$$C_p(m, v) = G(a_{\rm vap}/a)\pi a^2 v n_f(a) a \,, \qquad (33)$$

where $a_{\rm vap}$ is the radius of a field grain at the complete vaporization threshold, and function G is defined by

$$G(x \equiv a_{\rm vap}/a) = \int_0^x \frac{(1+t)^2\, dt}{t^{p-3}(1+t^3)}$$
$$= \frac{(1+x^{-3})x^{4-p}}{4-p}\left[1 + \frac{2(4-p)}{5-p}\,x + \frac{4-p}{6-p}\,x^2 - \frac{4-p}{7-p}\,x^3 - \frac{2(4-p)}{8-p}\,x^4 + \ldots\right]. \qquad (34)$$

The series solution is valid for $p \neq 4$ and converges rapidly because generally $a_{\rm vap} \ll a$ for partially vaporizing collisions. The effective destruction rate for partially vaporizing collisions, evaluated with the help of equations (33) and (34) for $p = 3.5$, is typically 3 times as large as the rate for completely vaporizing collisions.

The rate of fragment production in catastrophic collisions is less than destruction rate C, since C includes the complete and partial vaporization of the grain material. It can therefore be found by subtracting from C the rate for completely vaporizing collisions C_c, and that fraction of partial vaporizations that occur during catastrophic collisions. The latter contribution can be found by setting the lower limit of integration in equation (32) to the catastrophic fragmentation threshold and using the expansion series solution (eq. [34]). The results are presented in Figure 8, where we plot the fragment production rate divided by $d\ln v/dt$, for grains with radii of 0.02 μm and 0.25 μm. The fragment production rate is approximately 75% of the grain destruction rate above the threshold for vaporization, this percentage being only weakly dependent on grain radii and their velocities, and it is of course equal to the grain destruction rate below the vaporization threshold. Thus, about one-fourth of the grain material is vaporized on average in catastrophic collisions, and the remaining three-fourths is deposited into fragments.

For collisions below the catastrophic fragmentation threshold, but above the threshold for vaporization (i.e., for $v > 30$ km s^{-1}), the effective vaporization rate can be found by setting the upper limit of integration in equation (32) to the catastrophic fragmentation threshold and again using the series expansion solution (eq. [34]). The vaporization in such collisions reduces the amount of fine dust ejected in cratering events. In Figure 2, we plot the production rate of fine dust (divided by $d\ln v/dt$), for grains with radii of 0.02 μm and 0.25 μm. The fine dust production rate is 17% lower than the grain cratering rate for our standard model parameters, but this is offset by the reduced role of sputtering because a smaller amount of fine dust particles undergoes sputtering following their ejection from a crater. Therefore, the total amount of dust mass returned to the gas phase in cratering collisions (Figs. 6 and 7) is not affected by partial vaporizations.

3.4. *Combined Effects of Grain Erosion, Fragmentation, and Vaporization*

The grain destruction processes just described redistribute grain mass into tiny dust particles ejected from craters and larger fragments resulting from catastrophic fragmentation and transform solid material into gas through sputtering and vaporization. Just as was done in § 3.1 for erosion and sputtering alone, we can now describe this redistribution process more fully by taking into account catastrophic fragmentations.

The mass in surviving grains can be found by following the grain along its trajectory in $\{m, v\}$ space, from its initial mass m_0 at v_0 to its final mass m_f at rest, and then multiplying m_f by $\exp(-\tau_0)$ (τ_0 is the optical depth for grain destruction). The mass fraction in surviving grains is then $\exp(-\tau_0)$ times smaller than shown in Figure 7, with τ_0 as plotted in Figure 9. We show this fraction in Figures 11 and 12 for a large ($a_0 =$

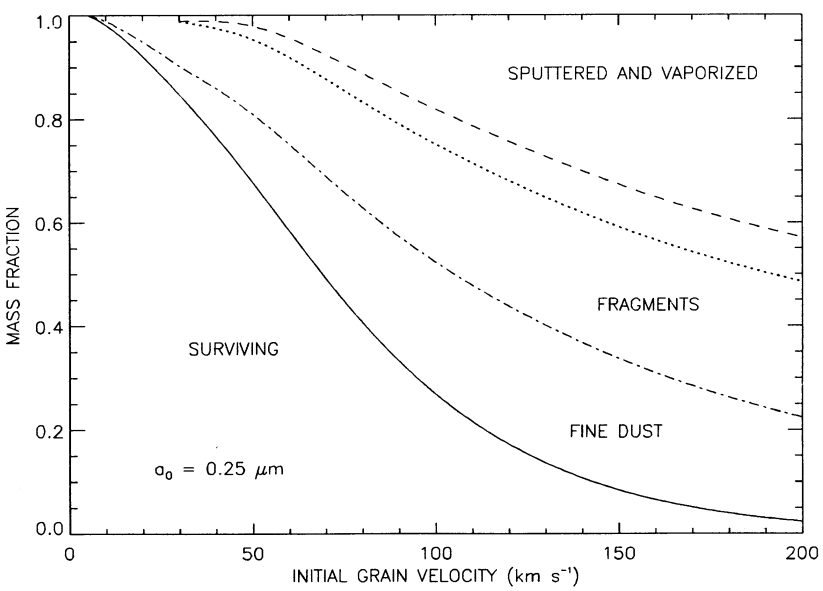

FIG. 11.—The relative distribution between sputtered and vaporized grain mass, mass deposited in small dust particles and in bigger catastrophic fragmentation products, and the final mass in surviving grains, for the initial grain radius $a_0 = 0.25$ μm. The sputtered and vaporized mass fraction includes vaporization in catastrophic collisions (the region between dotted and dashed lines). Erosion and destruction of fragments is not included.

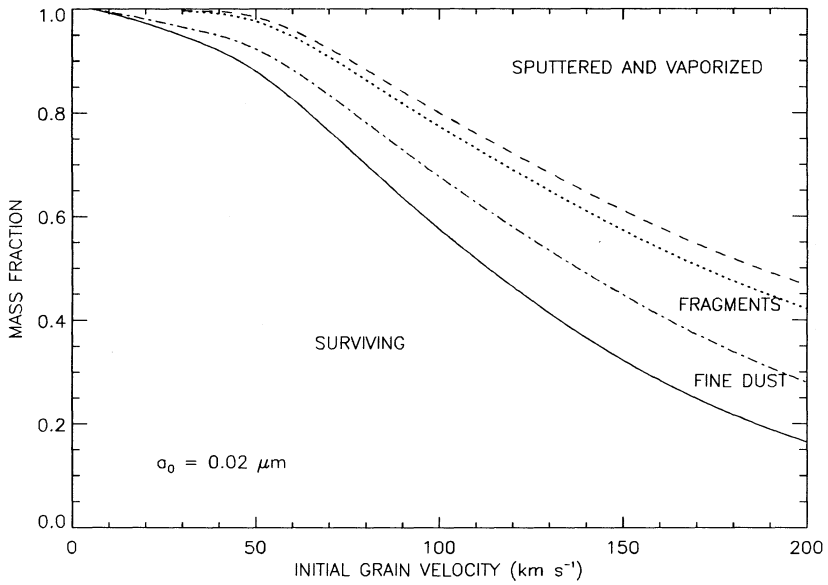

FIG. 12.—Same as Fig. 11, but for small grains ($a_0 = 0.02$ μm)

0.25 μm) and a small ($a_0 = 0.02$ μm) grain, respectively. By comparing with Figure 7, it can be seen that large grains are particularly strongly affected by catastrophic collisions. Half the grain mass is lost at velocities as low as 70 km s^{-1} for the initial grain size of 0.25 μm, and only 2.5% remains if the grain started with $v_0 = 200$ km s^{-1}. This further reinforces our conclusion about the effectiveness of the large grain destruction in g-g collisions. At large velocities, most of the grain mass is removed through sputtering and cratering; relative contributions of sputtering, vaporization, and cratering (resulting in the production of fine dust particles) are also plotted in the figures. These contributions were evaluated by integrating relevant rates along the grain trajectories, as in § 3.1, but these rates were weighted by $\exp(\tau - \tau_0)$ in order to take into account destruction of grains by catastrophic collisions.

The fraction of mass removed by catastrophic fragmentations can be found by evaluating the integral $\int_0^{\tau_0} m(\tau) \exp(\tau - \tau_0) d\tau/m_0$, where $m(\tau)$ is the grain mass along its trajectory in $\{m, \tau(v)\}$ space. The result is shown in Figures 11 and 12 as the region between dotted and dash-dotted lines. As shown in § 3.3, approximately one-fourth of the grain mass removed by catastrophic collisions is vaporized, except at low velocities. This is depicted by dotted lines in Figures 11 and 12, where the region between dashed and dotted lines is the mass fraction vaporized in catastrophic collisions. The mass deposited into fragments is still an appreciable fraction of the grain mass over a large range in velocities, particularly for larger grains. Note that the mass fraction deposited into fragments is not equal to the final mass in surviving fragments, because fragments also undergo erosion and destruction as they are slowing down. The fate of fragments depends on their size distribution and will be discussed next.

4. THE EVOLUTION OF THE FRAGMENT SIZE DISTRIBUTION

4.1. *Rate Equations for Grain Size Distribution*

Let $n(m, v, t)dmdv$ be the number density of dust fragments in the mass interval $(m, m + dm)$ with velocities between v and $v + dv$. The equation describing the evolution of $n(m, v, t)$ in a homogeneous medium is given by

$$\frac{\partial n(m, v, t)}{\partial t} = -\frac{\partial \dot{m} n(m, v, t)}{\partial m} - \frac{\partial \dot{v} n(m, v, t)}{\partial v} - C(m, v) n(m, v, t) + K(m, v \mid m_b, v_b) n_b + \int_m^{m_{\max}} \int_0^{\infty} n(\mu, u, t) K(m, v \mid \mu, u) du d\mu \, . \quad (35)$$

The first term on the right-hand side of this equation represents grain erosion caused by cratering and sputtering, with the (negative) erosion rate $\dot{m} = \dot{m}_s + \dot{m}_{cr}$ being the sum of the sputtering and cratering rates. We discussed these rates in § 2 (see eqs. [3] and [12]). The second term on the right-hand side describes how the fragment population evolves in the presence of the net acceleration $\dot{v}$ on dust grains, which is given by equation (14). These two terms together form the divergence of the grain flux in $\{m, v\}$ space; without subsequent terms on the right-hand side equation (35) would simply be a conservation law for the grain number density in the divergence form. In accordance with our discussion in § 3.1, we neglected diffusion across grain trajectories caused by the stochastic nature of the cratering process.

The next three terms on the right-hand side of equation (35) account for catastrophic g-g collisions; they are an equivalent of the collision integral on the right-hand side of the collisional Boltzmann equation. In the third term on the right-hand side, $C(m, v)$ is the removal rate of grains with mass m and velocity v resulting from complete vaporization and catastrophic fragmentation, given by equation (23). The two source terms (fourth and fifth terms in eq. [35]) represent fragments with masses m and velocities v, which are produced in catastrophic collisions and which must be added to the distribution function. Fragments may be produced either in disruptions of primary (beam) grains, with mass $m_b(t)$, velocity $v_b(t)$, and number density $n_b(t)$ (see § 3.2) leading to creation of "primary" fragments (fourth term), or in the subsequent fragmentation cascade (fifth term). In the latter case, the double

integration must be performed over fragment velocities u and over grain masses larger than m. Both source terms do not include the fine fragments produced in cratering events. The function $K(m, v \mid \mu, u)dmdv$ is the probability (s^{-1}) that fragments with masses $(m, m + dm)$ and velocities $(v, v + dv)$ will be produced in a disruption of a grain with mass μ and velocity u. It can be written as

$$K(m, v \mid \mu, u) = \int_{m_{\rm thr}}^{m_{\rm max}} n_f(\mu')u\sigma(\mu, \mu')f(m, v \mid \mu, u, \mu')d\mu' , \quad (36)$$

where $f(m, v \mid \mu, u, \mu')$ is the fragmentation function discussed in § 2.4. If, according to the discussion presented there, velocities of fragments are set to zero in the frame of reference moving with the center of mass velocity $v_c = \mu u/(\mu + \mu')$ of colliding grains, then fragments with velocities between v and $v + dv$ result from collisions with stationary field grains with masses between $\mu' = \mu(u/v - 1)$ and $\mu' + d\mu' = \mu(u/v - 1) - (\mu + \mu')^2 dv/\mu u$. Equation (36) then becomes

$$K(m, v \mid \mu, u) = n_f(\mu')\sigma(\mu, \mu')f(m \mid \mu, u, \mu')(\mu + \mu')^2/\mu , \quad (37)$$

with f given by equation (10) and $\mu' = \mu(u/v - 1)$. In the limit of high grain velocities, the fast-moving grain is disrupted mostly in collisions with much smaller grains, and a useful approximation for K is

$$K(m, v \mid \mu, u) = \delta(v - u) \times \int_{m_{\rm thr}}^{m_{\rm max}} n_f(\mu')u\sigma(\mu, \mu')f(m \mid \mu, u, \mu')d\mu' , \quad (38)$$

because fragments are then injected into the gas with velocity v nearly equal to u.

We solved rate equation (35) using a combination of analytical and numerical methods described in the Appendix. Briefly, this equation was solved analytically by an iterative method analogous to a hierarchy solution of the Boltzmann equation. Fragments were divided into "primary" fragments resulting from shattering of beam dust grains, "secondary" fragments resulting from shattering of "primary" fragments, and subsequent fragment generations. The result for the number density n_0 of primary fragments,

$$n_0(m) = \int_0^{\tau_0} \exp\,[-\tau(m_0, v_b)]n_b f(m_0 \mid m_b)\frac{dm_0}{dm}\,d\tau_b , \quad (39)$$

has a simple interpretation. The destruction rate of beam grains in the optical depth interval $(\tau_b, \tau_b + d\tau_b)$ along their trajectory is equal to $n_b\,d\tau_b$. The production rate of fragments with mass m_0 is found by multiplying this rate by the fragmentation function $f(m_0 \mid m_b)$. The optical depth $\tau(m_0, v_b)$ measures the destruction of these fragments through the exponential term in equation (39). Finally, the derivative dm_0/dm measures the shift and distortion of the distribution function caused by fragment erosion. The integration over velocities has been replaced by integration along the beam particle path. Equation (39), with the help of equation (31), can also be written as

$$n_0(m) = n_{b0}\exp(-\tau_0) \times \int_0^{\tau_0} \exp\,[\tau(m_b, v_b) - \tau(m_0, v_b)]f(m_0 \mid m_b)\frac{dm_0}{dm}\,d\tau_b . \quad (40)$$

While the primary fragment distribution can be easily obtained from these equations by a simple numerical integration, the solution for subsequent fragment generations is considerably more difficult, as described in the Appendix.

4.2. *Results*

The primary fragment size distribution depends on the slope chosen for the fragmentation function, and the initial grain radius and velocity. The distribution has the same slope at small fragment sizes as the fragmentation function; small fragments are unlikely to be destroyed in catastrophic collisions because of their small optical depths for grain destruction, while sputtering and cratering merely grind them to smaller sizes without changing the slope of the distribution. Note that this result is very different than in cratering collisions, since we found a strong excess of small to large fragments in cratering collisions (§ 2.5). This result is intuitively obvious because smaller grains are expected to be produced predominantly in more frequent and less energetic cratering events rather than in rare catastrophic collisions.

There are two major departures from the distribution assumed for the fragmentation function. First, the primary fragment size distribution is noticeably steeper, particularly for grains with large initial velocities. Second, the maximum fragment size is significantly smaller than the initial grain radius. For example, for the initial grain radius of 0.25 μm and the initial velocity of 200 km s^{-1} (and $p = 3.5$), we find the maximum fragment radius to be equal to 0.10 μm. At this fragment radius, the primary fragment size distribution is down by a factor of 3.5 relative to the MRN distribution, normalized at small fragment sizes. These departures from the MRN distribution may be traced to the destruction of fragments through sputtering, cratering, vaporization, and catastrophic fragmentation, as they slow down to rest following the breakup of the parent grain. Just as for beam grains, these effects are less pronounced for smaller parent grains; if we take the initial grain radius of 0.02 μm instead of 0.25 μm, the maximum fragment radius is equal to 0.012 μm, and the reduction in the primary fragment distribution is only 30%.

The mass fraction in primary fragments is shown in Figure 13 as a function of the initial grain velocity, for a number of grain radii. Also plotted is the mass fraction initially deposited in fragments, as shown in Figures 11 and 12. The difference between the final mass fraction and the fraction initially deposited into fragments is caused by destruction of fragments as they slow down to rest. This destruction is not nearly as effective as the destruction of the beam grains, but the mass fraction in surviving primary fragments is much reduced for high grain velocities.

The contribution of secondary fragments to the total fragment population is expected to be most significant for large beam grains with high initial velocities because of their large optical depths for grain destruction (Fig. 9). In Figure 14, we plot the secondary fragment size distribution for large beam grains, 0.25 μm in size, injected with the initial velocity of 200 km s^{-1}. Also shown is the primary fragment size distribution, and the sum of primary and secondary fragments. The secondary fragment distribution is obviously steeper than the primary fragment distribution, which was already shown to be steeper than the MRN distribution assumed for the fragmentation function. The maximum radius of secondary fragments is also less than that of primary fragments. Such steepening of the distribution function and the reduction in the maximum fragment size are expected in the fragmentation cascade, as fragments are broken into smaller and smaller pieces. The total

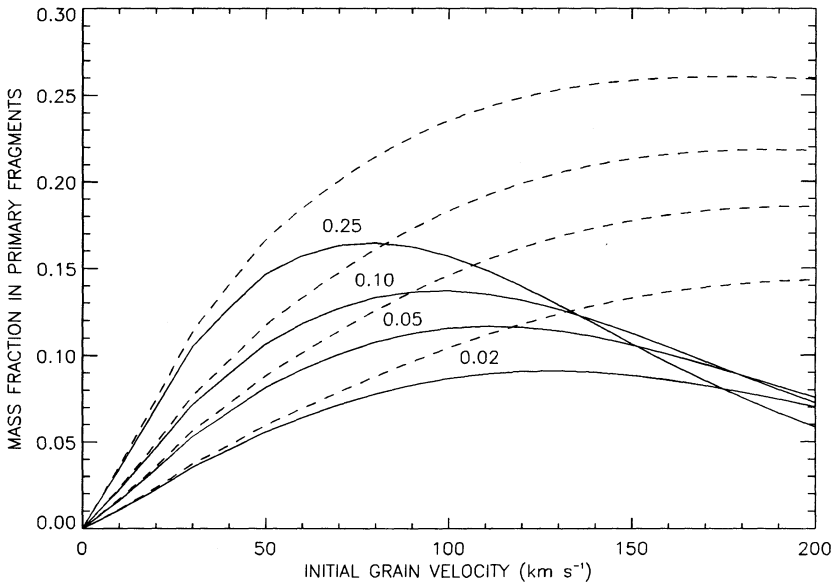

FIG. 13.—Mass fraction in primary fragments vs. *initial* grain velocity (*solid lines*). This fraction is less than the total mass fraction initially deposited in fragments (*dashed lines*) because of the fragment erosion and destruction. Curves are labeled by the *initial* grain radius (μm).

mass in secondary fragments larger than 0.005 μm is equal to 1.5% of the initial beam grain mass, about 25% of the mass contained in primary fragments. This modest contribution brings the total mass in surviving fragments to over 7% by mass. As seen in Figure 14, the contribution of secondary fragments is substantial at small fragment radii, making the total fragment distribution much steeper than the MRN distribution. (The effective power-law index p of the distribution shown in Fig. 14 is equal to 4 in the size range from 0.005 μm to 0.1 μm.)

While results presented in Figure 14 demonstrate that production of secondary fragments is important for the largest grains with high velocities, we find that secondary fragments contribute little to the total fragment population throughout most of our parameter space. For example, the production rate of secondary fragments for 0.25 μm beam grains injected with 100 km s^{-1} is virtually identical to the case discussed above, in terms of the total mass contained in secondary fragments. However, this comprises less than 10% of the mass contained in primary fragments. Nearly as large a reduction in relative production of secondary fragments occurs if, instead of decreasing the initial beam grain velocity from 200 km s^{-1} to 100 km s^{-1}, we decrease the initial beam grain radius from 0.25 μm to 0.10 μm. We conclude that for our model parameters (Table 1) the production of secondary fragments is important only for large ($a_0 > 0.2$ μm) grains with initial velocities near or in excess of 200 km s^{-1}. The subsequent fragment generations are, of course, of even less significance.

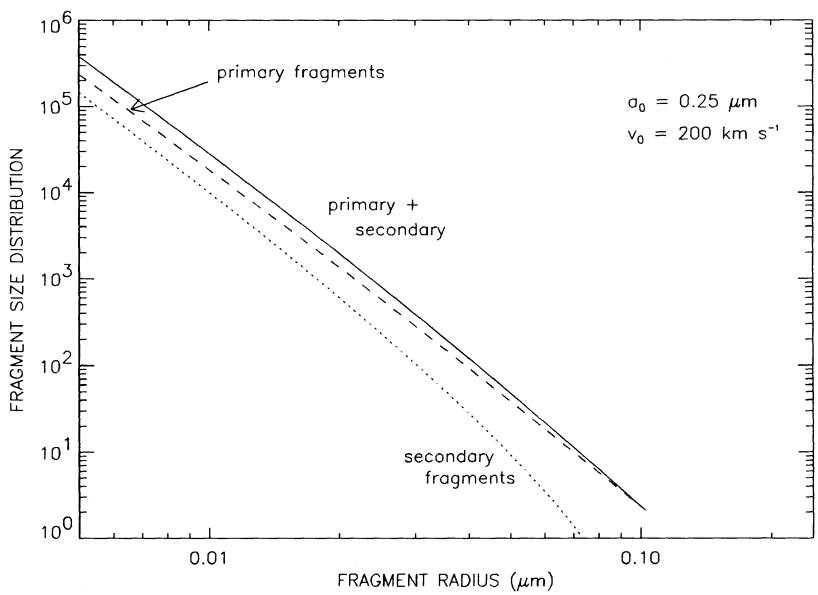

FIG. 14.—Size distribution of fragments created from $v_0 = 200$ km s^{-1}, $a_0 = 0.25$ μm beam grains. The secondary fragment distribution (*dotted curve*) is steeper than the primary fragment distribution (*dashed curve*) and contributes noticeably to the total fragment population at small grain radii.

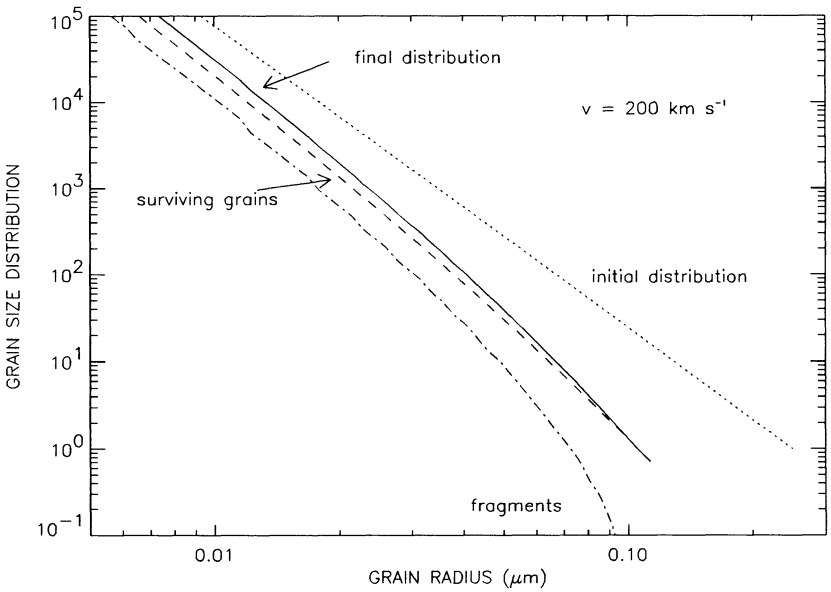

FIG. 15.—Evolution of grain size distribution, starting from an initial MRN distribution moving with velocity of 200 km s^{-1}. The final distribution (*solid curve*) is the sum of surviving grains (*dashed curve*) and fragments (*dash-dotted curve*). Note the difference in slopes and the maximum grain size between the initial (*dotted curve*) and the final distributions.

Interstellar dust consists of grains with a continuous distribution of sizes, so that we should also consider a continuous distribution of beam grain sizes. Consider then an ensemble of beam grains with the MRN grain size distribution, injected with the initial velocity v into an ambient, dusty medium. What is the final distribution of these beam grains and their fragments after they have been decelerated? On the basis of calculations reported above, we can now provide an answer to this question. First, the beam grains undergo grain erosion and grain destruction through catastrophic fragmentations. This will shift the initial distribution to smaller grain sizes and reduce the grain number density. Because large grains are more susceptible to processing by g-g collisions, the final distribution of surviving grains is expected to be steeper than the original distribution. This is demonstrated in Figure 15, in which we show the results for $v = 200$ km s^{-1}. Also shown is the fragment size distribution and the final grain size distribution, which includes both fragments and surviving grains. (In accordance with the discussion presented above, only primary fragments are taken into account; we neglected a small contribution from subsequent fragment generations.) This distribution is much steeper than the orignal MRN distribution; the effective power-law index in the 0.01–0.1 μm grain radius range is equal to 4.4, instead of 3.5. Grain destruction is clearly accompanied by steepening of the grain size distribution and a reduction in the maximum grain size. These effects are, of course, less pronounced at lower velocities, as demonstrated in Figure 16 for grains with initial velocities of 100 km s^{-1}.

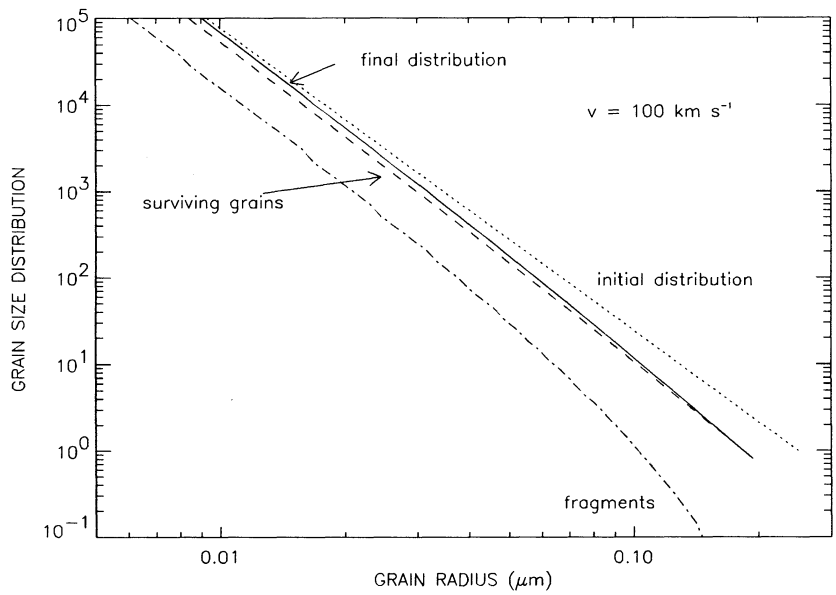

FIG. 16.—Same as Fig. 15, but for velocity of 100 km s^{-1}

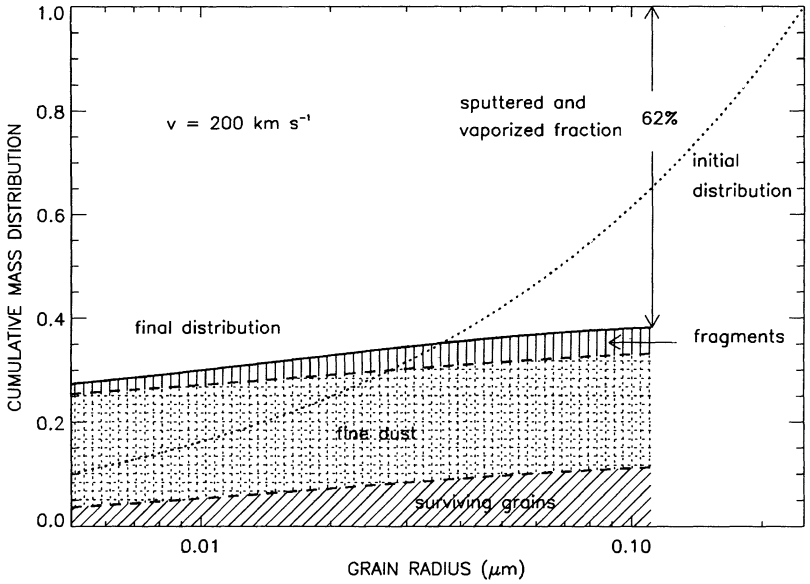

FIG. 17.—Cumulative mass distribution, starting from an initial MRN distribution (*dotted curve*) moving with velocity of 200 km s^{-1}. Most material in solid phase, which escaped sputtering or vaporization, was deposited into fine ($a < 0.005$ μm) dust.

We would like to emphasize that a significant fraction of the beam grain mass is deposited into fine dust. Its importance can be seen in Figures 17 and 18, in which we show the cumulative mass distribution (the total mass contained in grains smaller than radius a, normalized to the mass of the initial distribution) corresponding to distributions shown in Figures 15 and 16, respectively. For a high velocity of 200 km s^{-1} (Fig. 17), the fine ($a < 0.005$ μm) dust is the dominant component of grains which survived sputtering and vaporization. However, even at 100 km s^{-1} (Fig. 18), the fine dust constitutes a sizable fraction of the total grain mass, comparable to the sputtered and vaporized fraction. The steepening and a reduction in the maximum grain size seen in Figures 15 and 16 is thus accompanied by an efficient production of fine dust grains.

The grain mass redistribution strongly depends on the injection velocity of an initial MRN distribution of grain sizes. This is shown in Figure 19, in which we plot the fractional mass in various dust components for the two cases discussed above, with injection velocities of 100 km s^{-1} and 200 km s^{-1}, and for an additional case with 50 km s^{-1}. The height of each bar gives the grain mass which escaped sputtering or vaporization. While only several percent of the dust mass was returned to gas at 50 km s^{-1}, the sputtered and vaporized mass fraction increased to 64% at 200 km s^{-1}. This is accompanied by a pronounced reduction in the mass fraction of surviving original dust grains. More than half the grain mass was processed for the initial velocity of 100 km s^{-1}, and a scant 11% survived at 200 km s^{-1}. In addition to sputtering and vaporization, the

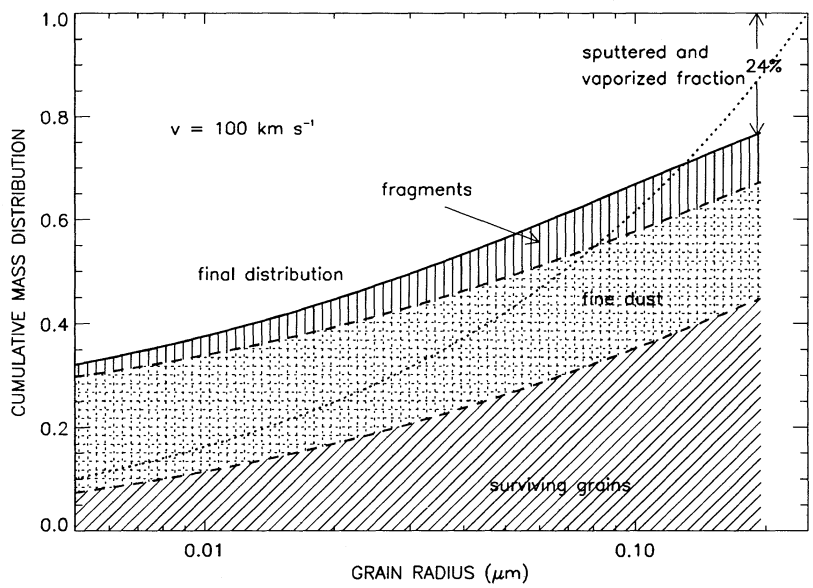

FIG. 18.—Same as Fig. 17, but for velocity of 100 km s^{-1}

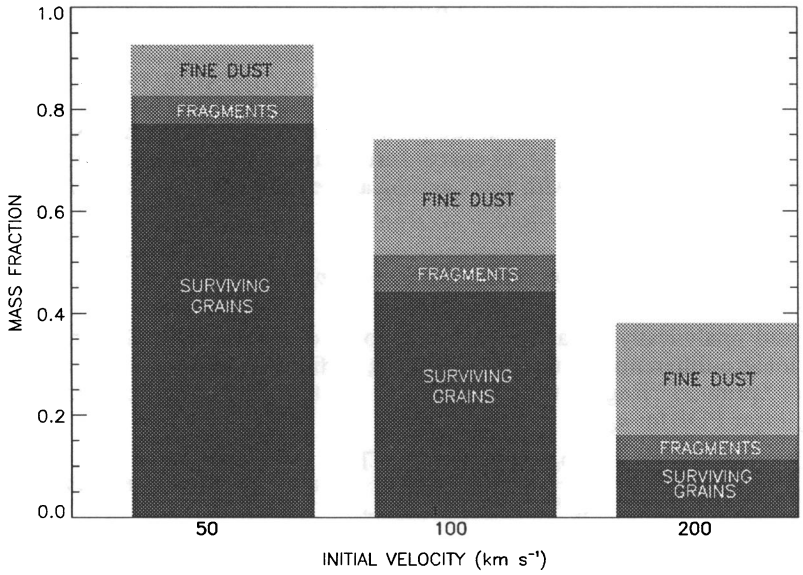

FIG. 19.—Final grain mass redistribution vs. grain initial velocity, for an initial MRN distribution of grain sizes. The height of each bar gives the grain mass which escaped sputtering or vaporization. Note strong dependence on the initial grain velocity and a high efficiency of fine dust production across the whole velocity range.

processed grain mass ended mostly in fine dust particles. The production rate of larger ($a > 0.005$ μm) fragments is modest, less than 10% of the grain mass, depending weakly on the injection velocity in the range from 50 km s^{-1} to 200 km s^{-1}.

5. SUMMARY

In this paper we studied the various grain destruction processes operating on fast-moving dust particles slowing down in a dusty gas. We divided these processes into two categories: continuous processes, sputtering and cratering, that result in the gradual erosion of the dust particle; and catastrophic processes, vaporization and fragmentation, that result in the total disruption of the dust particle. The rate of grain erosion resulting from sputtering and cratering, respectively, is given by equations (3) and (11). Catastrophic processes are characterized by a threshold velocity for their occurrence and effectiveness (see §§ 2.3 and 2.4).

The destruction of grains by continuous processes can be described by a trajectory in the $\{m, v\}$ plane, where m is the mass of the dust particle and v is its velocity. Both m and v are gradually decreasing from some initial value $\{m_0, v_0\}$ as the dust particle is gradually eroded and decelerated by the ambient gas. Figure 4 describes the trajectories of dust particles for various initial values of $\{m_0, v_0\}$ as they slow down by collisional drag in a dusty gas. The relative importance of these two processes depends on the initial grain velocity and size and is shown in Figure 3. Figure 7 summarizes the fraction of the initial mass of a dust particle that is eroded in the form of fine dust particles by cratering collisions and the fraction that is returned to the gas phase by sputtering, as a function of initial grain size and velocity.

At any point along the trajectory, a dust particle may be subjected to a catastrophic collision, which will terminate the particle trajectory. The probability for such an event is equal to $1 - \exp(-\tau)$, where τ is a function of grain mass and velocity along the trajectory. The parameter τ is an effective optical depth with which we can measure the diminution of a beam of dust particles moving through a dusty gas. Figure 9 presents the optical depth for grain destruction by a catastrophic collision. A catastrophic collision terminates the trajectory of the original particle in $\{m, v\}$ space and generates new trajectories for the fragments created in the collision. These trajectories may also terminate with a catastrophic collision, generating new fragment trajectories as well. The cascade continues until the velocity of the original dust particle or any of its "offspring" fragments slow down to velocities below the threshold for any grain destruction process. The dust particle then becomes a "field" particle, which may be further destroyed by catastrophic collisions with fast-moving "test" particles. This cascade of grain destruction and fragment generation was cast as an integro-differential equation in § 4.1, and the numerical solution was described in § 4.2. The evolution of the distribution of grain sizes, initially characterized by a power law following their injection in a dusty gas, is presented in Figures 17 and 18. Figure 19 depicts the final mass redistribution of a population of fast-moving dust particles initially characterized by an MRN size distribution. The figures show that in contrast to population of dust particles subjected to thermal sputtering, the final grain size distribution is characterized by an excess of small relative to large particles, compared to the initial size distribution. Small dust particles are stochastically heated by the ambient radiation field, generating an excess of short-wavelength IR emission over that expected from larger dust radiating at the equilibrium dust temperature. Grain destruction by grain-grain collisions should therefore have an observable signature that can be characterized by a correlation between the short-to-long wavelength IR emission and shock velocity. Such correlation has already been hinted at by observations of intermediate velocity molecular clouds (Heiles et al. 1988).

We would like to thank Mike Shull for an illuminating discussion and for many useful comments following his thorough reading of our manuscript.

APPENDIX

SOLUTION OF RATE EQUATIONS FOR GRAIN SIZE DISTRIBUTION

Rate equation (35) is a linear, partial integro-differential equation for $n(m, v, t)$, with fragments moving along trajectories given by equations (14) and (15), and shown in Figure 4 in $\{a, v\}$ space. Just as in the case of the Boltzmann equation, it is convenient to transform equation (35) to its Lagrangian form, with the Lagrangian derivative defined as $D/Dt = \partial/\partial t + \dot{m}\partial/\partial m + \dot{v}\partial/\partial v$. Along each grain trajectory,

$$\frac{Dn(m, v, t)}{Dt} = -\left[\frac{\partial \dot{v}}{\partial v} + \frac{\partial \dot{m}}{\partial m} + C(m, v)\right] n(m, v, t) + K(m, v \mid m_b, v_b) n_b(t) + \int_m^{m_{\max}} \int_0^{\infty} n(\mu, u, t) K(m, v \mid \mu, u) du d\mu \, . \tag{A1}$$

Equation (A1) can be solved analytically by a method analogous to a hierarchy solution of the Boltzmann equation. We transform the linear, partial integro-differential equation (A1) into an infinite set of partial differential equations (PDEs). First, we denote the number density of "primary" fragments, resulting from shattering of beam dust grains, by $n_0(m, v, t)$. From equation (A1), we obtain the following linear PDE for n_0:

$$\frac{Dn_0(m, v, t)}{Dt} = -\left[\frac{\partial \dot{v}}{\partial v} + \frac{\partial \dot{m}}{\partial m} + C(m, v)\right] n_0(m, v, t) + K(m, v \mid m_b, v_b) n_b \, . \tag{A2}$$

Next, we denote number densities of subsequent fragment generations by $n_i(m, v, t)$. Their evolution along each grain trajectory is given by

$$\frac{Dn_i(m, v, t)}{Dt} = -\left[\frac{\partial \dot{v}}{\partial v} + \frac{\partial \dot{m}}{\partial m} + C(m, v)\right] n_i(m, v, t) + \int_m^{m_{\max}} \int_0^{\infty} n_{i-1}(\mu, u, t) K(m, v \mid \mu, u) du d\mu \tag{A3}$$

for $i = 1, \infty$. The infinite set of linear PDEs (A2) and (A3), with

$$n(m, v, t) = \sum_{i=0}^{\infty} n_i(m, v, t) \, , \tag{A4}$$

is equivalent to the rate equation (A1).

Linear PDEs (A2) and (A3) can be reduced to quadratures. Let

$$F(m, v, t) \equiv \int_{t_0}^{t} \left\{\frac{\partial \dot{v}}{\partial v} + \frac{\partial \dot{m}}{\partial m} + C[m(t'), v(t')]\right\} dt' \, , \tag{A5}$$

where the integration is performed along a grain trajectory, from (m_0, v_0) at a reference time t_0 to (m, v) at time t. The number density $n_0(m, v, t)$ of primary fragments is then

$$n_0(m, v, t) = \exp(-F)\left\{n_0(m_0, v_0, t_0) + \int_{t_0}^{t} K[m(t'), v(t') \mid m_b, v_b] n_b \exp(F) \, dt'\right\} . \tag{A6}$$

But

$$\exp(-F) = (\det \boldsymbol{J})^{-1} \exp[\tau(m, v) - \tau(m_0, v_0)] \, , \tag{A7}$$

where $\boldsymbol{J}(t)$ is the Jacobian of the transformation from the grain mass m_0 and its velocity v_0 at reference time t_0 to its mass m and velocity v at time t, whose determinant measures volume changes in $\{m, v\}$ space along the grain trajectory, while $\tau(m, v)$ is the optical depth for grain destruction along this trajectory, defined by equation (30). We can then write equation (A6) as

$$n_0(m, v, t) = [\det \boldsymbol{J}(m, v, t)]^{-1} \exp[\tau(m, v) - \tau(m_0, v_0)]\left\{n_0(m_0, v_0, t_0) + \int_{t_0}^{t} K(m, v \mid m_b, v_b) n_b \det \boldsymbol{J}(t') \exp[\tau(m_0, v_0) - \tau(m, v)] dt'\right\} . \tag{A8}$$

Similarly,

$$n_i(m, v, t) = [\det \boldsymbol{J}(m, v, t)]^{-1} \exp[\tau(m, v) - \tau(m_0, v_0)]\left\{n_i(m_0, v_0, t_0) + \int_{t_0}^{t} \int_m^{m_{\max}} \int_0^{\infty} n_{i-1}(\mu, u, t) K(m, v \mid \mu, u) du d\mu \det \boldsymbol{J}(t') \exp[\tau(m_0, v_0) - \tau(m, v)] dt'\right\} , \tag{A9}$$

where the integrations in t' in equations (A8) and (A9) are again performed along the same trajectory as in equation (A5), passing through (m_0, v_0) at t_0 and (m, v) at t.

The fragment number density $n(m, v, t)$ can now be found iteratively, first by solving for n_0 from equation (A8), they by using equation (A9) to find n_i for $i = 1, 2, \ldots$, and finally by summing all n_i values according to equation (A4). This iterative scheme

converges quickly for small optical depths τ; n_i becomes negligible in comparison with the lower members of the series in equation (A4) after several iterations. In addition, by relatively simple quadratures, we obtain not only the total number density of fragments, but also the relative contribution of subsequent fragment generations. Our hierarchical, iterative method is expected to break down for fast-moving large grains when the optical depth for grain destruction is much larger than one. In the asymptotic limit of $\tau \to \infty$, the grain will be fragmented into a multitude of very small fragments. This is the regime of the extreme dust destruction, where most of the grain material is expected to be returned to the gas phase.

Equation (A8) for the number density of primary fragments assumes a particularly simple form in the limit of high grain velocities, when the function K can be approximated by equation (38). In this case, the integral in equation (A8) is equal to zero, because fragments with mass m and velocity v are produced only at the intersection of their trajectory with the trajectory of beam grains at time t_0. The fragment velocity at this intersection is equal to the velocity $v_b(t_0)$ of beam grains. The number density of primary fragments at time t_0 is

$$n_0(m_0, v_b, t_0) = -\frac{C(m_b, v_b) n_b f(m_0 \mid m_b)}{(a_b/a_0 - 1)\, dv_b/dt} = \frac{n_b f(m_0 \mid m_b)}{(a_b/a_0 - 1)} \frac{d\tau_b}{dv_b}, \tag{A10}$$

so that the number density $n_0(m, v, t)$ of primary fragments at any time t is then

$$n_0(m, v, t) = [\det \boldsymbol{J}(m, v, t)]^{-1} \exp [\tau(m, v) - \tau(m_0, v_0)] \frac{n_b f(m_0 \mid m_b)}{(a_b/a_0 - 1)} \frac{d\tau_b}{dv_b}, \tag{A11}$$

according to equation (A8). This explicit expression is particularly useful in calculations of the next (secondary) fragment generation from equation (A9).

We are particularly interested in finding the primary fragment distribution, integrated over velocities, at large times t when fragments are at rest. This can be done by integrating equation (A11) over velocities and noting that $\tau(m, v) \to 0$ for large t. The result,

$$n_0(m) = \int_0^{\tau_0} \exp [-\tau(m_0, v_b)] n_b f(m_0 \mid m_b) \frac{dm_0}{dm} d\tau_b, \tag{A12}$$

with the help of equation (31), can also be written as

$$n_0(m) = n_{b0} \exp (-\tau_0) \int_0^{\tau_0} \exp [\tau(m_b, v_b) - \tau(m_0, v_b)] f(m_0 \mid m_b) \frac{dm_0}{dm} d\tau_b. \tag{A13}$$

In the limit of high grain velocities, when function K can be approximated by equation (38), equation (A9) for the number density of subsequent fragment generations simplifies to

$$n_i(m, v, t) = [\det \boldsymbol{J}(m, v, t)]^{-1} \exp [\tau(m, v) - \tau(m_0, v_0)] \times \int_{t_0}^{t} \int_{m(t')}^{m_{\max}(t')} n_{i-1}(\mu, v, t) C(\mu, v) f(m \mid \mu) d\mu \det \boldsymbol{J}(t') \exp [\tau(m_0, v_0) - \tau(m, v)]\, dt'. \tag{A14}$$

Note that except for the primary fragments, fragment densities at the intersection of their trajectories with that of the beam grains are equal to zero. Equation (A14) completes our formal solution for the evolution of the fragment size distribution.

The rate equations for the grain size distribution discussed above are in general difficult to solve numerically, even with a formal reduction to quadratures accomplished above. The numerical solution becomes somewhat easier in the limit of high grain velocities when function K can be approximated by equation (38). Because our efforts are focused on fast-moving grains, we take advantage of this approximation. The primary fragment size distribution is then given by equation (A13), which can be easily evaluated numerically by standard integration algorithms. We calculated the primary grain size distribution according to equation (A13), with the fragmentation function given by equation (10). Our standard value for parameter x in this equation is 0.833, corresponding to the power-law index $p = 3.5$ of the fragment size distribution (Table 1). According to our discussion in § 3.3, approximately one-fourth of the grain mass removed by catastrophic collisions is vaporized, except at low velocities. Therefore, above the threshold for vaporization ($v > 30$ km s^{-1}), we set s in equation (10) equal to 0.75, so that the maximum fragment size is 90.9% of the original grain size. Below the vaporization threshold, we adopted a nearly identical fragmentation function, with the same maximum fragment size, but with the total fragment mass equal to the mass of the disrupted grain.

The numerical calculation of subsequent fragment generations according to equation (A14) is substantially more difficult. Its solution for the secondary ($i = 1$) fragment generation requires first the evaluation of the primary fragment distribution n_0 as a function of fragment mass μ, its velocity v, and time t according to equation (A11). The next step involves the nontrivial multiple integration of n_0 as given by equation (A14), followed by an additional integration of $n_1(m, v, t)$ over velocities to obtain the final distribution of secondary fragments as a function of their mass m at $t \to \infty$. Instead of performing these integrations directly using equation (A14), we found it more convenient to integrate the original PDE (A3) along each grain trajectory, using standard ordinary differential equation solvers. Our solution strategy is then to evaluate n_0 according to equation (A11), perform a quadrature over primary fragments to obtain the source term for production of secondary fragments (second term on right-hand side of eq. [A3]), numerically integrate equation (A3) for $n_1(m, v, t)$, and then integrate n_1 over velocities. Because our results show that the fragment population is strongly dominated by the primary fragments in most cases, with the subsequent fragment generations contributing only a small fraction of the total mass contained in fragments, we provide here only a brief sketch of our solution method,

highlighting the most salient points. For the same reasons, we terminated our calculations at the second fragment generation, although our solution method can be in principle used to find the number density of subsequent fragment generations.

The evaluation of n_0 from equation (A11) requires the knowledge of det $\boldsymbol{J}$, the fragment and beam grain masses (radii) at the intersection of their trajectories where the fragment was produced, the location of the intersection, and the difference in optical depths from the current location of the fragment to this intersection. All these quantities can be found by solving a set of ordinary differential equations (ODEs) along the fragment trajectory. A coupled set of three ODEs for the fragment and the beam grain radii, and for the fragment velocity, was integrated as a function of the beam grain velocity from the current time t backward, until the fragment velocity was equal to the beam grain velocity. (We used an ODE solver SDEROOT from a public domain package ODE to accomplish this task.) Instead of solving for the volume changes in $\{m, v\}$ space along the fragment trajectory, as measured by det $\boldsymbol{J}$, and for the optical depth difference along the trajectory, we solved directly for function F (eq. [A5]) along the trajectory and then used equation (A7) in combination with equation (A11) to evaluate n_0. After finding n_0, we evaluated and stored in a tabular form the source function for production of secondary fragments, using the same fragmentation function as for the primary fragments. This task is also nontrivial because of the variable integration rage (as explicitly noted in eq. [A14]) and requires a solution of a two-point boundary value problem involving the set of three ODEs mentioned above. With the source function known, we integrated equation (A3) along the fragment trajectory, starting at the intersection with the beam grain trajectory at which the number density n_1 of secondary fragments must vanish. The final integration over the velocity distribution of secondary fragments completed our numerical calculations.

REFERENCES

Allamandola, L. J., Tielens, A. G. G. M., & Barker, J. R. 1985, ApJ, 290, L25
Baines, M. J., Williams, I. P., & Asebiomo, A. S. 1965, MNRAS, 130, 63
Barlow, M. J. 1978a, MNRAS, 183, 367
———. 1978b, MNRAS, 183, 397
———. 1978c, MNRAS, 183, 417
Barlow, M. J., & Silk, J. 1977, ApJ, 211, L83
Biermann, P., & Harwit, M. 1980, ApJ, 241, L105
Bohdansky, J. 1984, Nucl. Instrum. Methods Phys. Res., B2, 587
Burke, J. R., & Silk, J. 1974, ApJ, 190, 1
Campbell, E. E. B., Schyja, V., Ehlich, R., & Hertel, I. V. 1993, Phys. Rev. Lett., 70, 263
Cleveland, C. L., & Landman, U. 1992, Science, 257, 355
Cowie, L. L. 1978, ApJ, 225, 887
Draine, B. T., & Anderson, N. 1985, ApJ, 292, 494
Draine, B. T., & Salpeter, E. E. 1979a, ApJ, 231, 77
———. 1979b, ApJ, 231, 438
Dwek, E. 1986, ApJ, 302, 363
Dwek, E., & Arendt, R. G. 1992, ARA&A, 30, 11
Dwek, E., Foster, S., & Vancura, O. 1994, ApJ, submitted
Dwek, E., & Scalo, J. M. 1979, ApJ, 233, L81
———. 1980, ApJ, 239, 193
Fujiwara, A., Cerroni, P., Davis, D., Ryan, E., Di Martino, M., Holsapple, K., & Housen, K. 1989, in Asteroids II, ed. R. P. Binzel, T. Gehrels, & M. S. Matthews (Tucson: Univ. of Arizona Press), 240
Hartmann, W. K. 1969, Icarus, 10, 201
Heiles, C., Reach, W. T., & Koo, B.-C. 1988, ApJ, 332, 313
Hellyer, B. 1970, MNRAS, 148, 383
———. 1971, MNRAS, 154, 279
Holsapple, K. A. 1993, Annu. Rev. Earth Planet. Sci., 21, 333
Itoh, H. 1989, PASJ, 41, 853
Jones, A. P., Tielens, A. G. G. M., Hollenbach, D. J., & McKee, C. F. 1994, ApJ, 433, 797
Jura, M., & Kroto, H. 1990, ApJ, 351, 222
Katakuse, I., Baba, S., Ichihara, T., & Ikeya, M. 1992, Japanese J. Appl. Phys., 31, 1245
Leger, A., & Puget, J. L. 1984, A&A, 137, L5
Liffman, K. 1990, ApJ, 355, 518
Mathis, J. S., Rumpl, W., & Nordsieck, K. H. 1977, ApJ, 217, 425 (MRN)
Mathis, J. S., & Whiffen, G. 1989, ApJ, 341, 808
McKee, C. F. 1989, in IAU Symp. 135, Interstellar Dust, ed. L. J. Allamandola & A. G. G. M. Tielens (Dordrecht: Kluwer), 431
McKee, C. F., Hollenbach, D. J., Seab, C. G., & Tielens, A. G. G. M. 1987, ApJ, 318, 674
Melosh, H. J. 1989, Impact Cratering: a Geologic Process (New York: Oxford Univ. Press)
Melosh, H. J., Ryan, E. V., & Asphaug, E. 1992, J. Geophys. Res., 97, 14735
O'Keefe, J. D., & Ahrens, T. J. 1982, J. Geophys. Res., 87, 6668
Schulte, J. 1995, Phys. Rev. B, 51, 3331
Seab, C. G., & Shull, J. M. 1983, ApJ, 275, 652
Shull, J. M. 1977, ApJ, 215, 805
———. 1978, ApJ, 226, 858
Sigmund, P. 1981, in Sputtering by Particle Bombardment, ed. R. Behrisch (Berlin: Springer-Verlag), 9
Spitzer, L. 1976, Comments Astrophys., 6, 157
Tielens, A. G. G. M., McKee, C. F., Seab, C. G., & Hollenbach, D. J. 1994, ApJ, 431, 321
Vancura, O., Raymond, J. C., Dwek, E., Blair, W. P., Long, K. S., & Foster, S. 1994, ApJ, 431, 188
Zeldovich, Ya. B., & Raizer, Yu. P. 1967, Physics of Shock Waves and High-Temperature Hydrodynamic Phenomena (New York: Academic Press)